RESEARCH ARTICLE

Ten-year chemical signatures associated with long-range transport observed in the free troposphere over the central North Atlantic

B. Zhang[*,†], R. C. Owen[*,‡], J. A. Perlinger[*], D. Helmig[§], M. Val Martín[‖], L. Kramer[*,¶], L. R. Mazzoleni[*] and C. Mazzoleni[*]

Ten-year observations of trace gases at Pico Mountain Observatory (PMO), a free troposphere site in the central North Atlantic, were classified by transport patterns using the Lagrangian particle dispersion model, FLEXPART. The classification enabled identifying trace gas mixing ratios associated with background air and long- range transport of continental emissions, which were defined as chemical signatures. Comparison between the chemical signatures revealed the impacts of natural and anthropogenic sources, as well as chemical and physical processes during long transport, on air composition in the remote North Atlantic. Transport of North American anthropogenic emissions (NA-Anthro) and summertime wildfire plumes (Fire) significantly enhanced CO and O_3 at PMO. Summertime CO enhancements caused by NA-Anthro were found to have been decreasing by a rate of 0.67 ± 0.60 ppbv/year in the ten-year period, due possibly to reduction of emissions in North America. Downward mixing from the upper troposphere and stratosphere due to the persistent Azores-Bermuda anticyclone causes enhanced O_3 and nitrogen oxides. The $d[O_3]/d[CO]$ value was used to investigate O_3 sources and chemistry in different transport patterns. The transport pattern affected by Fire had the lowest $d[O_3]/d[CO]$, which was likely due to intense CO production and depressed O_3 production in wildfire plumes. Slightly enhanced O_3 and $d[O_3]/d[CO]$ were found in the background air, suggesting that weak downward mixing from the upper troposphere is common at PMO. Enhancements of both butane isomers were found during upslope flow periods, indicating contributions from local sources. The consistent ratio of butane isomers associated with the background air and NA-anthro implies no clear difference in the oxidation rates of the butane isomers during long transport. Based on observed relationships between non-methane hydrocarbons, the averaged photochemical age of the air masses at PMO was estimated to be 11 ± 4 days.

Keywords: Long-range transport patterns to Azores; Long-term observations of ozone and ozone precursors; Non-methane hydrocarbon aging

1. Introduction

The central North Atlantic Ocean is a remote region where transport of pollutants from North America, Europe, and Africa has been observed. The meteorology in this region is usually controlled by a persistent mid-latitude anticyclone, known as the Azores-Bermuda High. Its strength and location change seasonally and interannually, causing synoptic transport patterns to vary, bringing air masses from different continents. There has been much effort to study the tropospheric chemistry and long-range transport over the North Atlantic. In the 1990s, the North Atlantic Regional Experiment (NARE, (Fehsenfeld et al., 1996)) was conducted to investigate transport of CO and O_3 from North America. It was found that transport of air pollutants has a significant influence on air composition over the North Atlantic Ocean. During the International Consortium for Atmospheric Research on Transport and Transformation (ICARTT, Fehsenfeld et al., 2006) experiment, observations including ground and aircraft measurements were collected over North America, the Azores and Europe to study the impacts of long-range transport crossing the North Atlantic. The more recent BORTAS campaign focused on remarkable long-range transport of wildfire emissions to the North Atlantic (Parrington et al., 2012). The majority of the studies for

* Atmospheric Sciences, Michigan Technological University, Houghton, US

† National Institute of Aerospace, Hampton, US

‡ Environmental Protection Agency, Research Triangle Park, US

§ Institute of Arctic and Alpine Research, University of Colorado, Boulder, US

‖ Chemical and Biological Engineering, University of Sheffield, Sheffield, UK

¶ University of Birmingham, Birmingham, UK

Corresponding author: B. Zhang (bzhang3@mtu.edu)

the North Atlantic Ocean focused on transport events or short-term observations. The chemical climatology and the roles of different transport patterns have not been discussed based on long-term observations.

Pico Mountain Observatory (PMO), in the Azores, Portugal, is an island site established in 2001 for the purpose of studying North American outflow (Honrath et al., 2004). The elevation of PMO is 2225 m asl, so the site allows monitoring long-range transport in the free troposphere for most of the time. Tracer gases have been observed at PMO since 2001. Data collected until now provide precious long records that are very useful to investigate different transport patterns and the impacts on air composition over the central North Atlantic.

Studies of chemical transformation during transport can rely on relationships of simultaneously-observed chemicals in downwind regions. $d[O_3]/d[CO]$ (the linear regression slope between O_3 and CO concentrations) has been used as a measure of O_3 enhancement in downwind regions of continental sources (e.g., Parrish et al., 1993). Variations in the slope observed in previous studies reflected differences in air composition and differing O_3 chemistry. A $d[O_3]/d[CO]$ value of 0.3 was found to be a signature value for rural sites in eastern North America, and was concluded to be a result of mixing of fresh pollution emissions and aged air mass (Chin et al., 1994). Cooper et al. (2001) investigated $d[O_3]/d[CO]$ in different airstreams associated with mid-latitude cyclones, and suggested that the slope could be different depending on air composition and photochemistry. Honrath et al. (2004) found a higher summertime $d[O_3]/d[CO]$ (~1.0) in the free troposphere over the central North Atlantic and suggested potential O_3 production during transport from North America. A previous study (Zhang et al., 2014) investigated the evolution of $d[O_3]/d[CO]$ during selected transport events of pollution plumes from North America to PMO in a semi-Lagrangian view, using data from PMO and a chemical transport model. It was found that photochemical CO loss can also contribute to increases in $d[O_3]/d[CO]$ in long-range transport, so the higher $d[O_3]/d[CO]$ at PMO compared to places closer to emission sources (i.e., over the U.S.) were due to not only photochemical ozone production but also CO loss. For the comparisons of $d[O_3]/d[CO]$ at a given location, such as PMO, the differences in CO loss for pollution impacted transport should not be significant. Zhang et al. (2014) estimated 10% and 12% CO loss due to photochemistry for two transport events of polluted plume having significant different OH concentrations and transport pathways. Thus, differences in observed $d[O_3]/d[CO]$ at PMO should mainly reflect varying emission strength and ozone chemistry for the pollution impacted transport.

Non-methane hydrocarbons (NMHC) mainly undergo reactions with OH radicals in the troposphere, and their relative reaction ratios are useful tools to determine the photochemical age of transported air masses. Lighter NMHC usually react more slowly than heavier ones. Consequently, concentrations of lighter NMHC are still measurable after long-range transport. The differences in NMHC decay rates produce specific patterns in the observed mixing ratios, which have been used to reflect photochemical ages of air masses (Mckeen and Liu, 1993). The natural logarithm of [n-butane]/[ethane] versus that of [propane]/[ethane] has been used as a photochemical clock of air masses (Parrish et al., 1992). The butane isomer ratio, [i-butane]/[n-butane], has been used to investigate oxidation pathways by OH, ocean-emitted chlorine atom, and other oxidants (Hopkins et al., 2002).

In this work, a ten-year record of trace gas observations at PMO was used to study relationships between air composition and transport patterns. The objectives of this work are to provide a classification of major transport patterns to PMO that are characterized by different pollution sources and transport pathways, and to investigate the associated chemical signatures. We investigated O_3 and O_3 precursors in spring (April and May), summer (June, July and August) and fall (September and October). We only focused our analyses on months from April to September, because data from PMO were most available during the periods.

2. Methods
2.1. PMO measurements and research
PMO was established in the summer of 2001 on top of Pico Mountain (38.47° N, 28.40° W, 2225 m a.s.l.) in the Azores Islands, Portugal. The elevation of PMO in the central North Atlantic ocean makes it an excellent site for conducting research on gaseous and particle species transported in the free troposphere. Since the establishment of PMO, studies have been conducted to understand the impacts of pollution transport, photochemistry, and meteorology on the air composition at this baseline site. Honrath et al. (2004) and Owen et al. (2006) focused on CO and O_3 observations in the earlier years, and specifically investigated the enhancements due to transport from North America. Both Lapina et al. (2006) and Val Martín et al. (2006) studied impacts of fire emissions on enhancement of air pollutants at PMO. Val Martín et al. (2008b) focused on a three-year period of nitrogen oxides observation and studied the seasonal variations and sources of nitrogen oxides. Helmig et al. (2008) and Honrath et al. (2008) assessed NMHC levels observed at PMO, and used NMHC data to investigate oxidation chemistry and plume aging over the North Atlantic. Aerosol properties and composition have also been measured to investigate aerosol radiative effect and aging during long-range transport (Fialho et al., 2005; Dzepina et al., 2015; China et al., 2015). A recent work by Helmig et al. (2015) discussed observed seasonal cycles and the degree of photochemical aging of NMHC at PMO using data collected during 2004–2014. The study here uses ten years of measurements (2001–2010) of CO, O_3, nitrogen oxides ($NO_x = NO + NO_2$), total reactive nitrogen (NO_y), and NMHC to study the chemical signatures of different transport patterns (data coverage is shown in **Figure 1**). Data used in this work are archived at http://instaar.colorado.edu/pico/pico_archive/default.html. Details about the instrumentation of individual species are summarized in Honrath et al. (2004) (CO and O_3), Val Martín et al. (2006) (NO_x and NO_y), Kleissl et al. (2007) (meteorology), Tanner et al. (2006) (NMHC), and Helmig et al. (2008) (NMHC).
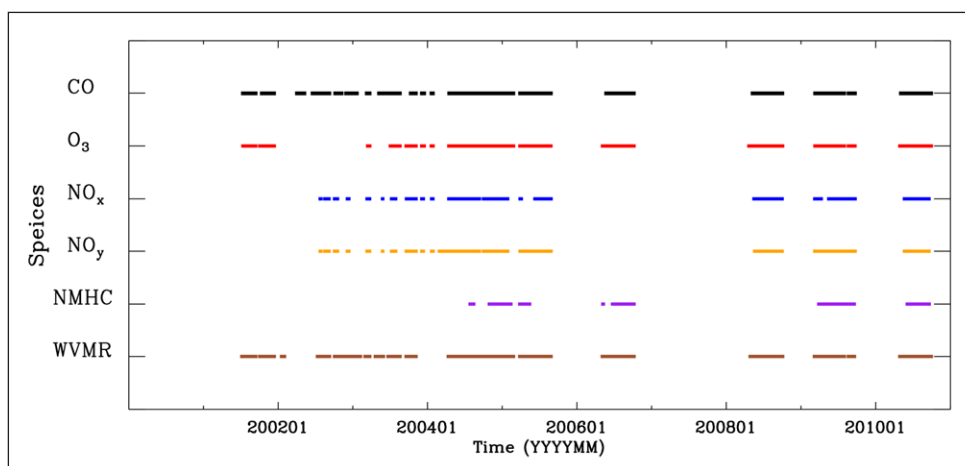
Zhang et al: Ten-year chemical signatures associated with long-range transport observed in the free troposphere over the central North Atlantic

Art. 8, page 3 of 20

Figure 1: Availability of trace gas observations at PMO during 2001–2010. DOI: https://doi.org/10.1525/elementa.194.f1

2.2. Transport and CO tracer simulations

The Lagrangian particle dispersion model FLEXPART (version 8.2; (Stohl et al., 1998)) was used to build a ten-year archive of transport trajectories for PMO. Backward simulations were launched every three hours from PMO. Meteorology fields from the European Center for Medium-Range Weather Forecasting (ECMWF), featured with 3-hourly temporal resolution, 1° horizontal resolution, and 60 vertical levels, were used to drive simulations for 2001–2004. Meteorology fields of the Global Forecast System (GFS) and its Final Analysis (FNL), featured with the same temporal and horizontal resolutions, but 26 vertical levels, were used to drive FLEXPART for the years 2005–2010. The output was saved in a grid with a horizontal resolution of 1° latitude by 1° longitude, and eleven vertical levels from the surface to 15,000 m a.s.l. A "retroplume" obtained in FLEXPART backward simulations describes upwind distributions of residence time (introduced with details in supplemental information (SI)), which is a useful tool to study transport pathways. Retroplumes are multiplied with CO emission inventories from the Emissions Database for Global Atmospheric Research (EDGAR version 3.2 (Olivier and Berdowski, 2001)) and the Global Fire Emissions Database (GFED v3.1, daily averaged fire emissions (Mu et al., 2011)) to estimate influence from anthropogenic and wildfire sources, respectively. The product is hereafter called "FLEXPART_CO" (examples are given in Figure S1). It has been found that GFED v3.1 misses biomass burning emissions from small fires, but the bias due to such misses was estimated to be only 9% in annual total emissions in the temperate to boreal North America (Randerson et al., 2012). Not all of the missing emissions can be transported to PMO, so the chance of missing "Fire" events should be even lower and is believed to have minor impacts on the analyses in this work.

Uncertainties in transport pathways simulated by FLEXPART can be due to the parameterizations representing temporally and spatially unresolved transport processes (Stohl et al., 2011). In terms of vertical transport processes, boundary layer mixing and updrafts in convection are both considered in FLEXPART. Time-varying PBL height determines the vertical mixing of air parcels. Failure to capture the daily PBL peak can lead to overestimation of surface concentrations. In FLEXPART, PBL height is calculated using the Richardson number concept based on the wind and temperature fields given in the meteorology (Vogelezang and Holtslag, 1996). The meteorology fields used in this work had a temporal resolution of 3 hours, and at least one local afternoon time was included. Sub-grid variables, including topography and land use, can also affect vertical mixing. Oversimplified topography may overlook shear stress and sensible heat, creating biases in vertical distributions of tracers. Another highly parameterized sub-grid process is cloud convection. FLEXPART redistributes air parcels vertically in convection-activated grids using the approach of Emanuel and Emanuel and Zivkovic-Rothman (1999), which determines air parcel displacement in up- and down-drafts based on temperature and humidity fields. The convection scheme is not necessarily the same scheme used in driving meteorology. These parameterizations have been fully tested and validated using surface and in situ measurements (Stohl et al., 1998; Brioude et al., 2013); therefore we do not believe that these associated uncertainties are significant enough to change the conjectures and conclusions of this paper.

2.3. Classification of transport patterns

In this section, we list the constraints used to determine different transport patterns. Helmig et al. (2015) also studied long-term transport patterns to Pico in different seasons by using HYSPLIT modeling. They found that fast transport was associated with shorter photochemical ages as indicated by observed ln[propane]/[ethane]. Here, we intend to further explore the transport types. By analyzing FLEXPART products and meteorological data, we identified several major transport patterns in the ten-year record of trace gas observations. The constraints are discussed in the following and summarized in **Table 1**.

2.3.1. Air mass origin

The primary consideration in categorizing the transport is where it originates. We considered transports originating from North America, Europe and Africa, downward mixing from the upper troposphere and lower stratosphere (UTLS), and North Atlantic background air. Transport origin was determined based on the distributions of upwind residence

Art. 8, page 4 of 20

Zhang et al: Ten-year chemical signatures associated with long-range transport observed in the free troposphere over the central North Atlantic

Table 1: Constraints to define transport patterns, abbreviations of the transport patterns, and the estimated occurrence frequencies in spring (April and May), summer (June, July, and August), and fall (September and October). DOI: https://doi.org/10.1525/elementa.194.t1

Transport Patterns	Abbrev.	Constraint*	Occurrence Frequency ** %		
			Spring	Summer	Fall
North American flow	NA	RT over North America in 0–5 km a.s.l. greater than 50% for at least 1 day	40	30	32
NA affected by anthropogenic emissions	NA-anthro	North America anthropogenic FLEXPART_CO contribution greater than 15 ppbv, fire <15 ppbv	16	15	13
NA-anthro lifted during transport	NA-anthro-lifted	1. Same as NA-anthro	4.0	2.7	2.5
		2. RT in a vertical range 0–2.5 km reduced 30% within 24 hour during 0–15 days upwind			
NA-anthro within or close to MBL	NA-anthro-low	1. Same as NA-anthro	3.1	1.7	<1.0
		2. RT within 0–2.5 km greater than 40% from 0–5 days upwind			
NA-anthro quick transport	NA-anthro-young	1. Same as NA-anthro	6.7	4.3	4.0
		2. FLEXPART_CO age from anthropogenic emissions less than 7 days			
NA-anthro aged transport	NA-anthro-aged	1. Same as NA-anthro	6.2	5.3	4.5
		2. FLEXPART_CO age from anthropogenic emissions greater than 10 days			
Wildfire affected	Fire	Wildfire FLEXPART_CO contribution greater than 15 ppbv, Anthropogenic <15 ppbv	<1.0	7.3	2.6
Fire quick transport	Fire-young	1. Same as Fire	<1.0	2.5	1.0
		2. FLEXPART_CO age from wildfire emissions less than 7 days			
Fire slow transport	Fire-aged	1. Same as Fire	<1.0	3.0	1.3
		2. FLEXPART_CO age from wildfire emissions greater than 10 days			
European flow	EU	RT over Europe greater than 50% for at least 1 day	1.8	<1.0	<1.0
African flow	AF	RT over Afreica greater than 50% for at least 1 day	<1.0	<1.0	2.6
North Atlantic free troposphere background	NATL	RT over North Atlantic in 0–5 km a.s.l. greater than 70% through 0–10 days upwind	17	19	8.3
Downward mixing from UTLS	Upper	RT less than 40% in 0–5 km through 2–12 days upwind	2.1	2.3	4.1
Upslope flow	Upslope	Simulated PBL height greater than altitude of Pico or DSL less than PBL height	24	13	15

* RT = residence time of FLEXPART retroplumes.

** Spring = April–May; Summer = June–August; Fall = September–October Unclassified time percentages are 22%, 39%, and 40 % for spring, summer, and fall, respectively.

time (RT) over the North Atlantic Ocean and the surrounding continents. **Figure 2a** provides the regional fraction of upwind RT averaged for all the retroplumes simulated for the ten years, which shows the averaged RT fractions in different regions at upwind days. During 0–3 days upwind, retroplume RT mainly distribute over the North Atlantic. The North American RT contribution started to appear between 1–2 days upwind, indicating the extreme shortest transport time from the North American continent to PMO. The average North American RT reached its maximum 7–8

days upwind at 22%. We defined the retroplumes that had greater than 50% RT distributed in the low-middle troposphere (0–5 km a.s.l.) over North America for a period longer than one day as "North American transport", with an assigned abbreviation of "NA". The altitude limitation was applied for targeting ground emissions because air originating from the upper troposphere would certainly have a different chemical composition. The upper limit of 5 km was set much higher than the typical boundary layer height to take into account surface air masses lofted by convec-
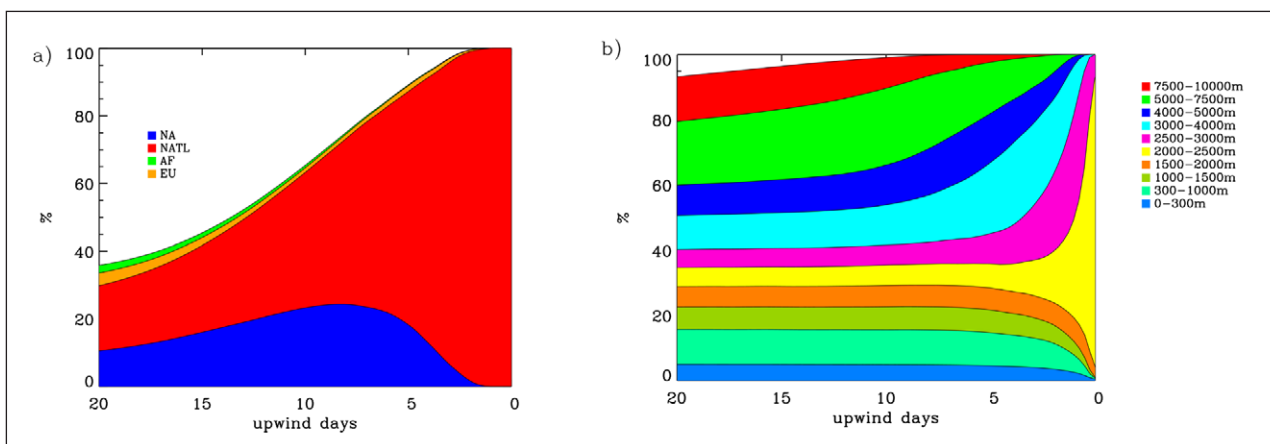
Zhang et al: Ten-year chemical signatures associated with long-range transport observed in the free troposphere over the central North Atlantic

Art. 8, page 5 of 20

Figure 2: Averaged upwind residence time distributions over different geographical regions **(a)** and vertical levels (%) **(b)** for 3 hourly retroplumes in 2010 simulated by FLEXPART. Note that not all transport sources and heights are included in the legends, and therefore total percentages are less than 100% in the upwind days. NA: North America; NATL: North Atlantic; AF: Africa; EU: Europe. DOI: https://doi.org/10.1525/elementa.194.f2

tion over continents. Using even higher levels (i.e., 7.5 km or 10 km) would have certainly captured deep convection but would also have increased the probability of including free troposphere air that was decoupled from surface emissions. The North Atlantic free troposphere background, "NATL", was constrained by a higher percentage (70%) of RT and a longer time limit (10 days) within 0–5 km a.s.l. over the North Atlantic in order to reduce the probability of overlapping with air masses originating from the continents. It is worth mentioning that we did not exhaustively classify all observations into a specific transport pattern. Instead, we determined the observations with clear transport characteristics and paid less attention to transport that had multiple origins and complicated pathways.

2.3.2. Impact of emission type and air mass age

FLEXPART_CO was used in this study to determine the periods when PMO was affected by two types of pollution emissions, i.e., anthropogenic and wildfire emissions (see details in SI). We used a FLEXPART_CO mixing ratio enhancement of 15 ppbv (compared to 80–100 ppbv as a typical background CO at PMO) as the cutoff in determining the periods affected by fresh emissions. For example, if FLEXPART_CO from biomass burning emission was greater than 15 ppbv for a particular time, then the period was considered as a fire event. The 15 ppbv used here equals the standard deviation of observed half-hourly CO for the ten-year period. We used the same anthropogenic emission inventory in FLEXPART for all the years in order to keep a consistent threshold for identification of affected periods, although the actual emissions of CO and reactive nitrogen oxides over North America have decreased in recent decades. The simulated FLEXPART_CO shows a wide range from 3 ppbv (small emission influence) to more than 150 ppbv (large emission influence). An example of FLEXPART_CO originating from different continents and types of emission is given in Figure SI1a.

FLEXPART_CO was also used to estimate the age of continental emissions after long-range transport by averaging the time elapsed between CO emission pick-up and the arrival at PMO in the model (see SI for details). Honrath et al. (2004) found that transport from North America that

causes significant changes in CO at PMO usually takes 5 to 7 days. Thus, we defined the transport retroplumes that had average FLEXPART_CO ages less than 7 days as short transport and those that were older than 10 days as aged transport. A one-month FLEXPART_CO age spectrum time series is shown in Figure SI1b for demonstration purpose. This constraint can be combined with the determined air mass origin to further distinguish transport patterns. For example, aged transport of North American anthropogenic emissions is referred to as "NA-anthro-aged". In previous work, this method was used to assess the influence of wildfire emission and transport pathway (Val Martín et al., 2008a; Dzepina et al., 2015; China et al., 2015).

2.3.3. Transport height

We also defined a few subcategories determined by transport at different heights or that experienced RT redistribution in height. Kleissl et al. (2007) reported that the MBL height at Pico was typically 800–1500 m simulated by the Global Data Assimilation System (GDAS, 2014). We studied the GDAS data again for the ten-year period and found the MBL occasionally reduced to 500 m or reached up to 2000 m. For such estimates, we defined a "low" transport pattern which had over 40% of its RT below 2.5 km during the transport period. This height was chosen because it was the first vertical level in the configured FLEXPART that reaches above 2 km. In order to capture the transport scenario, in which pollution emission was lifted by deep convection or by warm conveyor belts, we defined the "lifted" scenario when the RT was reduced by at least 30% in the 0–2.5 km within 24 hours during the simulated upwind transport. The fraction of RT change during lifting refers to the findings in a climatology study of warm conveyor belts over 15 years (Eckhardt et al., 2004). The last transport scenario defined by height was downward mixing, which brought air from the UTLS. Retroplumes having less than 40% of their RT within 0–5 km during 2–12 upwind days were defined as downward mixing having the abbreviation "Upper". In this definition, most of the air mass subsides from above 5 km to the level of PMO in the last few days of transport. The last two days were not considered because 100% of the RT should be at the

Art. 8, page 6 of 20

Zhang et al: Ten-year chemical signatures associated with long-range transport observed in the free troposphere over the central North Atlantic

level of PMO (2–2.5 km) when the simulated air parcels approached PMO as shown in **Figure 2b**.

2.3.4. Potential upslope flow

Local emissions from human activities and vegetation on Pico Island can be carried to PMO by upslope flow, which may lead to different chemical signatures. Upslope flow occurs through mechanically-forced lifting, in which strong synoptic winds blowing against the mountain are deflected upwards by the mountain slope, or through buoyant forcing, in which the surface air mass is lifted as a result of solar heating and release of latent heat. The frequency of upslope flow was found to be less than 20% at PMO from May to September by a micrometeorological study conducted during summertime in 2004 and 2005 (Kleissl et al., 2007). In our study, we examined potential upslope flow events for the ten-year period. For mechanically lifted upslope flow, the height of a dividing streamline (DSL) for the flow climbing upwards to PMO was calculated by using the method described in Sheppard (1956) and the wind speed profiles in the ECMWF and GFS/FNL meteorological datasets. DSL heights indicate the lowest level of air that can reach the top of Pico Mountain after consumption of the mechanical energy and, if any, latent heat. If the calculated DSL was lower than PBL height, upslope flow to PMO was considered as having occurred. We also considered deep convection caused by strong solar heating over the Island. We obtained PBL heights at PMO from GDAS (1° latitude by 1° longitude resolution) for the ten-year period and compared those with the height of PMO. When estimated PBL height exceeded the altitude of PMO, upslope flow was also considered as having occurred. In addition, we compared water vapor mixing ratios (WVMR) at PMO to the WVMR interpolated at the PMO elevation in the radiosonde measurements at Terceira (http://esrl.noaa.gov/raobs/). Similar to the approach used by Ambrose et al. (2011), we calculated the seasonal means of WVMR at 2225 m at the radiosonde site, Terceira. We determined, for each season, the driest portion of the PMO WVMR that derived equivalent seasonal means to the means at 2225 m above Terceira (within 0.01 g/kg). These subsets were considered as WVMR of free troposphere. The remaining data, and associated periods, were considered as anabatic upslope flows for each season, in addition to the two upslope flow situations determined above.

3. Results and discussions

3.1. Transport patterns and associated chemical signatures

The estimated occurrence frequencies of determined transport patterns are summarized in **Table 1**. The occurrence frequencies and chemical signatures for each transport pattern were calculated independently by applying the listed constraint(s) to the entire ten-year observations and model results. Thus, some categories are not exclusive. The largest data overlap between two transport patterns was less than 10% for NATL and Upper. The results are discussed together with observed chemical signatures in this section. We focus on the transport patterns with occurrence frequencies greater than 1%. The chemical signatures of trace gases determined for each transport pattern are summarized in **Table 2**. For the comparisons of chemical signatures in the following discussions, the Welch's t-test ($\alpha = 0.05$) was used to determine if the values were significantly different from each other.

3.1.1. North Atlantic free troposphere background

Figure 3a shows the superimposed RT of all the FLEXPART retroplumes classified as NATL in the ten-year period. The RT of NATL concentrated over the North Atlantic and was mostly isolated from continental emissions due to the constraints applied in Section 2. The occurrence frequencies of NATL were 17%, 19%, and 8.3% in spring, summer, and fall, respectively. The highest frequency in summer was likely due to the strengthened Azores-Bermuda anticyclone over the North Atlantic, which tends to constrain air to the central North Atlantic.

Due to the constraint implemented to classify NATL, we viewed this transport pattern as a flow of aged air that has been isolated from direct transport of continental sources for a long enough time such that the chemical signatures represent the background air composition of PMO. The average observed CO during NATL periods from the ten-year record were 113, 83, and 82 ppbv for spring, summer, and fall, respectively (**Table 2**). CO has a tropospheric lifetime of a few months, so the seasonal variations reflect the northern hemisphere seasonal CO background, which is driven by enhanced emission in cold seasons and accelerated oxidation in summer (Logan et al., 1981). Such maxima of CO in spring have been found at other remote sites (e.g., Macdonald et al. (2011) and for the Northern Hemisphere in general (Worden et al., 2013). The average O_3 of NATL were 39, 31, and 33 ppbv for spring, summer, and fall, respectively. These values are similar to the previously reported O_3 background at Bermuda (30–40 ppbv (Li et al., 2002)), but lower than the eastern U.S. mean O_3 in spring (47 ppbv) and summer (46 ppbv) (Cooper et al., 2012), reflecting an ozone destruction in the remote North Atlantic background air. The relatively lower O_3 in summer and fall, compared with spring, was likely the result of increased photochemical destruction of O_3 due to conversion of O_3 to OH when water vapor was more abundant. A springtime O_3 maximum has been found in multiple locations in the free troposphere. The causes of the maximum seem location dependent, and the roles of photochemistry, continental emissions, and transport from the stratosphere have been debated (Monks et al., 2000). Dry air conditions and weak radiation in early spring suppress HO_x production, which may lead to net ozone production in the low NO_x free troposphere (Yienger et al., 1999; Carpenter et al., 2000). The accumulation of NO_y and hydrocarbons due to longer lifetime in winter (e.g. PAN) has also been suggested as reasons for springtime O_3 peaks (e.g., Blake et al. (2003); Kramer et al. (2015)). Many studies have also reported impacts of downward transport from the stratosphere, e.g., Beekmann et al. (1994). Over the North Atlantic, Honrath et al. (1996) found that transport from the Arctic significantly increased ozone precursors during winter and spring.

Zhang et al: Ten-year chemical signatures associated with long-range transport observed in the free troposphere over the central North Atlantic

Art. 8, page 7 of 20

In contrast to CO and O_3, NO_x and NO_y for NATL had maxima in summer at PMO. We speculated that the strengthened Azores-Bermuda anticyclone and downward transport during summer could be the reason for summertime maxima of NO_y. NO_y in the middle and upper troposphere over oceans was found to be higher than within the marine boundary layer due to less efficient removal processes, including wet and dry deposition (Hübler et al., 1992). Talbot et al. (1999) investigated the NO_y budget during the NASA SONEX aircraft mission in the region and reported a median value of 0.17 for PAN/NO_y in the middle and upper troposphere. The downward transport could have brought NO_y to the lower troposphere in summer, and the thermal dissociation of PAN during subsidence could lead to increased NO_x. The coverage of NO_x and NO_y measurements was not as good as that of CO and O_3 due to technical difficulties at the site (**Figure 1**). Further analysis and chemistry modeling work need to be done to identify the quantification of background NO_x and NO_y. The characteristics of NATL downward transport will be discussed further in Section 3.2.1.

Table 2: Statistics of carbon monoxide (CO), ozone (O_3), nitrogen oxides (NO_x and NO_y), and NMHCs (ethane, n-propane, and n-butane) for the determined transport patterns in three seasons. The statistics are given in the form of mean ± standard deviation (number of observations). Values in bold font indicate the highest concentrations across all the transport patterns (highest in each row). Results of transport patterns that occur at a lower frequency than 1% (see **Table 1**) are not provided. DOI: https://doi.org/10.1525/elementa.194.t2

Species	Season	NATL	NA-anthro	NA-anthro-aged	NA-anthro-young	NA-anthro-lifted	NA-anthro-low
CO (ppbv)	Spring[1]	113±14(2160)	128±17(782)	121±12(630)	**131±17(753)**	128±19(580)	127±13(271)
	Summer	83±15(5284)	97±18(4077)	92±19(1580)	100±19(1042)	101±18(841)	100±17(454)
	Fall	82±15(1002)	105±15(1659)	100±15(554)	**111±14(590)**	108±14(446)	N.A.
O_3 (ppbv)	Spring	39±11(2533)	49±10(2323)	47±10(996)	50±10(762)	49±10(672)	44±9(311)
	Summer	31±11(6359)	41±12(4565)	40±14(1818)	41±12(1149)	42±12(925)	34±17(543)
	Fall	33±8(1201)	42±8(1928)	41±8(690)	45±7(640)	44±7(466)	N.A.
NO_x (pptv)	Spring	22±15(299)	48±39(206)	40±41(70)	52±36(79)	50±36(64)	N.A.
	Summer	51±51(1584)	52±43(1232)	51±38(465)	56±54(297)	52±37(210)	50±36(147)
	Fall	36±30(269)	39±23(324)	33±13(160)	N.A.[2]	40±20(90)	N.A.
NO_y (pptv)	Spring	132±121(621)	344±343(470)	276±176(167)	394±381(187)	**401±463(142)**	153±180(56)
	Summer	201±157(1651)	290±313(1266)	264±172(488)	277±334(301)	**314±296(236)**	157±127(147)
	Fall	111±109(275)	205±127(352)	182±123(161)	219±137(62)	218±90(101)	N.A.
Ethane (pptv)	Spring	1109±226(15)	1460±452(62)	1329±362(11)	1393±412(23)	**1483±490(18)**	N.A.
	Summer	523±224(66)	710±203(66)	587±187(27)	**792±199(20)**	N.A.	724±251(20)
	Fall	549±185(13)	878±192(27)	N.A.	**887±215(20)**	868±127(12)	N.A.
n-Propane (pptv)	Spring	130±50(35)	281±143(62)	173±82(11)	312±139(23)	**321±165(18)**	N.A.
	Summer	31±26(67)	82±55(68)	50±42(28)	114±55(21)	92±66(11)	N.A.
	Fall	90±82(26)	146±76(26)	N.A.	**148±87(19)**	137±53(12)	N.A.
n-Butane (pptv)	Spring	26±15(36)	60±43(63)	38±19(12)	61±35(23)	**65±46(19)**	N.A.
	Summer	14±12(56)	18±14(63)	15±11(24)	**23±14(21)**	**23±17(11)**	N.A.
	Fall	20±28(26)	23±15(27)	N.A.	23±16(20)	19±11(12)	N.A.
i-Butane (pptv)	Spring	11±6(36)	28±20(63)	15±11(12)	30±18(23)	**31±21(19)**	N.A.
	Summer	5±4(39)	9±6(57)	7±5(17)	10±6(21)	N.A.	8±6(17)
	Fall	N.A.	N.A.	N.A.	N.A.	N.A.	N.A.
WVMR (g/kg)	Spring	5.54±1.91(2394)	4.67±2.03(4512)	4.19±2.02(960)	5.26±1.94(797)	**4.66±1.66(729)**	6.37±1.34(340)
	Summer	6.98±2.61(5506)	6.71±2.81(4521)	6.00±2.87(1654)	7.21±2.91(1238)	6.56±2.69(914)	8.48±1.93(547)
	Fall	8.24±2.40(1069)	6.23±2.75(1877)	6.87±2.72(613)	5.46±2.61(667)	5.66±2.66(529)	8.22±1.77(252)

contd.

Art. 8, page 8 of 20

Zhang et al: Ten-year chemical signatures associated with long-range transport observed in the free troposphere over the central North Atlantic

Species	Season	Fire	Fire-aged	Fire-young	Upper	Upslope
CO (ppbv)	Spring	N.A.	N.A.	N.A.	123±11(206)	119±16(4141)
	Summer	**108±25(2296)**	107±20(885)	**108±32(538)**	92±16(655)	86±19(4642)
	Fall	N.A.	N.A.	N.A.	96±18(607)	86±17(2165)
O_3 (ppbv)	Spring	N.A.	N.A.	N.A.	**58±9(329)**	39±9(4787)
	Summer	47±13(2769)	45±11(968)	48±15(833)	**54±11(565)**	27±9(4650)
	Fall	42±12(63)	N.A.	N.A.	**49±8(635)**	32±7(2445)
NO_x (pptv)	Spring	N.A.	N.A.	N.A.	**63±47(82)**	37±38(591)
	Summer	59±35(542)	55±30(218)	60±44(137)	**66±65(129)**	48±52(1112)
	Fall	N.A.	N.A.	N.A.	**53±26(112)**	37±37(496)
NO_y (pptv)	Spring	N.A.	N.A.	N.A.	271±91(52)	150±183(1107)
	Summer	303±188(631)	265±152(259)	339±208(153)	234±69(127)	115±168(1106)
	Fall	N.A.	N.A.	N.A.	**229±85(113)**	73±79(492)
Ethane (pptv)	Spring	N.A.	N.A.	N.A.	N.A.	1256±320(174)
	Summer	773±225(19)	N.A.	N.A.	713±233(24)	626±229(74)
	Fall	N.A.	N.A.	N.A.	863±102(22)	672±288(37)
n-Propane (pptv)	Spring	N.A.	N.A.	N.A.	N.A.	196±102(175)
	Summer	**136±205(36)**	N.A.	N.A.	N.A.	58±46(75)
	Fall	N.A.	N.A.	N.A.	120±48(25)	90±58(59)
n-Butane (pptv)	Spring	N.A.	N.A.	N.A.	N.A.	42±28(170)
	Summer	22±25(34)	N.A.	N.A.	16±8(17)	16±11(68)
	Fall	N.A.	N.A.	N.A.	21±16(25)	28±21(58)
i-Butane (pptv)	Spring	N.A.	N.A.	N.A.	14±6(11)	19±14(170)
	Summer	**15±21(18)**	N.A.	N.A.	N.A.	11±15(67)
	Fall	N.A.	N.A.	N.A.	N.A.	12±8(58)
WVMR (g/kg)	Spring	5.78±2.38(80)	5.44±2.78(48)	6.29±2.48(32)	1.60±1.70(291)	**6.52±1.17(4141)**
	Summer	5.20±3.10(2214)	5.82±2.82(928)	4.70±3.13(801)	2.30±2.34(569)	**9.67±1.46(4642)**
	Fall	6.39±3.80(70)	3.02±3.62(27)	9.45±0.82(31)	3.06±2.83(713)	**9.48±1.50(2165)**

1. Spring: April and May; Summer: June, July and August; Fall: September, October.
2. N.A.: Results are not available because of lack of data and/or occurrence of the transport type is not frequent.

3.1.2. Transport affected by North American anthropogenic emissions

The transport affected by North American anthropogenic emission ("NA-anthro") had seasonal occurrence frequencies ranging from 13–16%. The integrated RT plot for NA-anthro (**Figure 3b**) shows a clear contribution from the northeastern states of the U.S. and a northwards curved transport pathway similarly to what has been found in previous North American transport events (Owen et al., 2006; Helmig et al., 2008, 2015). In the NA-anthro subsets, lifted transport ("NA-anthro-lifted") ranged from 2.5–4.0%, whereas the low altitude transport ("NA-anthro-low") had lower frequencies (1.0–3.1%). In terms of pollution age, transport older than 10 days ("NA-anthro-aged") occurred 4.5–6.2% of the time, whereas transport shorter than 7 days ("NA-anthro-young") ranged from 4.0 to 6.7%.

As a primary indicator of air pollution, CO enhancement (the amount that exceeds NATL) reflects the extent of pollution influence. North American anthropogenic emissions were estimated to add 15 ppbv (13%), 14 ppbv (17%), and 23 ppbv (28%) of CO to the background (NATL) in spring, summer, and fall, respectively (see **Table 2**). The larger percentiles in summer and fall were partly due to the low background of CO in the two seasons. In the NA-anthro sub-categories, CO for NA-anthro-low was statistically lower than the others; there was no significant difference among NA-anthro-lifted, -young, and -aged. The characteristic of NA-anthro-low was characterized by polluted air diluted by mixing with clean marine air within the MBL. Such findings suggest the mixing was more effective in reducing CO than photochemical aging in the transport from North America to PMO.
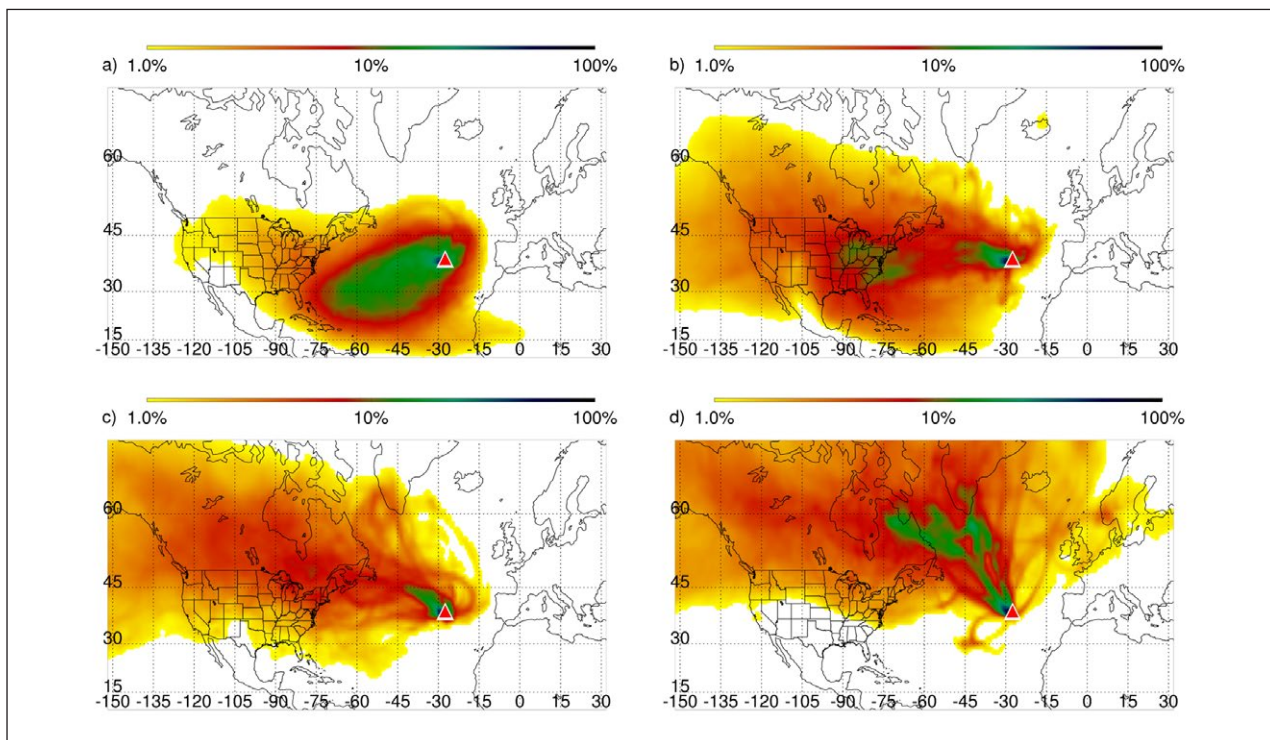
Zhang et al: Ten-year chemical signatures associated with long-range transport observed in the free troposphere over the central North Atlantic

Art. 8, page 9 of 20

Figure 3: FLEXPART simulated summertime column integrated residence time for determined transport patterns: **(a)** NATL, **(b)** NA-anthro, **(c)** Fire, and **(d)** Upper in 2001–2010. The color coding indicates the relative abundance of residence time. Abbreviations of the transport patterns are given in Table 1. DOI: https://doi.org/10.1525/elementa.194.f3

Ozone enhancements for the NA-anthro were 10 ppbv (25%), 10 ppbv (32%), and ppbv (30%) in spring, summer, and fall, respectively. The enhanced percentiles are different because the background levels were lower in summer and fall. As shown in **Table 2**, the mean O_3 mixing ratios in the NA-anthro sub-categories were all significantly different from each other, possibly suggesting O_3 levels were sensitive to transport heights and distances. The mean O_3 level of NA-anthro-low was lower than NA-anthro-lifted, which is a result of more efficient O_3 removal in low altitude transport and potential O_3 production by PAN decomposition in the subsidence stage of the lifted transport (Hudman et al., 2004; Zhang et al., 2014). The lower O_3 of NA-anthro-aged was generally due to the longer transport time and lack of O_3 precursor sources over the North Atlantic.

NO_x and NO_y levels at PMO were found to be driven by transport of pollution emissions, which was also discussed for a shorter measurement period by Val Martín et al. (2008a). Val Martín et al. (2008a) pointed out that summertime peaks of NO_y were caused by efficient transport of boreal wildfire emissions and pollution from eastern North America. Here, we find that the enhancements in NO_y caused by anthropogenic emissions were the highest in spring when the analysis was extended to the ten-year observation period. The springtime enhancements could be the result of less efficient wet deposition of NO_y and faster zonal transport in mid-latitude spring. The colder spring conditions could lead to a large contribution of PAN to NO_y in export from continental regions (Bey et al., 2001; Koike et al., 2003; Li et al., 2004), which

reduces the conversion from NO_y to HNO_3, and the following loss through wet deposition (Moxim et al., 1996). For the same reasons, NO_y for NA-anthro-lifted was much higher than that for NA-anthro-low due to accumulation of PAN and less efficient loss of NO_y at higher altitude. This transformation of NO_y has been studied in detail for two transport events to PMO by Zhang et al. (2014). NO_y of NA-anthro-low was lower than the other transport patterns, reflecting efficient removal of NO_y in the moist marine boundary layer air.

Maxima of NMHC were found during NA-anthro transport and its subcategories in spring and fall. During NA-anthro-lifted and NA-anthro-young transport, NMHC were higher than that of aged and low transport, suggesting that NMHC loss during transport is due to a combination of mixing with the background and chemical sinks through oxidation reactions with OH.

3.1.3. Trend analyses of CO and O_3 enhancements associated with NA-anthro

In order to understand the impacts of North American anthropogenic emissions in light of recent reductions of emissions, we calculated the annual variability in trace gas enhancements as shown in **Figure 4**. This analysis was only conducted for summer months, because CO observations were not adequate in spring and fall for a couple of years. As shown in **Figure 4**, we find a decreasing trend of CO enhancements (−0.67 ± 0.60 ppbv/yr as mean ± one-sigma error, *p*-value = 0.15) and no clear change of enhancements in O_3 (−0.04 ± 0.44 ppbv/yr, *p*-value = 0.47). These findings add on recent studies about CO
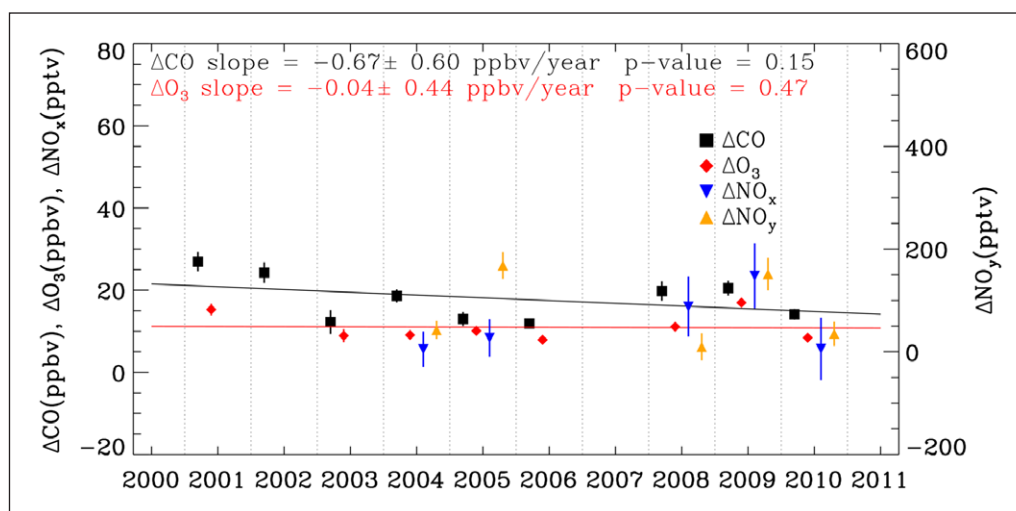
Figure 4: Trends of trace gas enhancements in transported North American anthropogenic emissions (NA-anthro minus NATL) in summer. The symbols represent the means of enhancements with vertical bars showing the 95% confidence intervals. The slopes were obtained from linear regression analyses for CO (black) and O_3 (red) enhancements. Slope ranges and *p* values are also shown in the figure. DOI: https://doi.org/10.1525/elementa.194.f4

trends in North American and globally. After the Environmental Protection Agency amended the Clean Air Act in 1990, air pollution emissions from the U.S. decreased (EPA, 2016). Globally-averaged CO has been found to have decreased at a rate of 1%/yr from 2001 to 2011 according to satellite observations (Worden et al., 2013). Trends of background O_3 in northern mid-latitudes have changed from positive to negative slopes around the year of 2000 (Parrish et al., 2012). In the eastern U.S., O_3 was found to have decreased at rates of –0.03 and –0.45 ppbv/year in spring and summer, respectively (Cooper et al., 2014). Previous work by Kumar et al. (2013) reported that both anthropogenic CO and NO_x emissions over the U.S. have decreased significantly since the beginning of the twenty-first century. The same study also found decreasing trends in CO (–0.31 ppbv/year) and O_3 (–0.21 ppbv/year) at PMO using a harmonic regression approach. The unclear trend in ozone enhancements in NA-anthro suggests that the decline in North American anthropogenic emissions was perhaps not significant enough to change ozone trends over the central North Atlantic. Instead, the decreasing trend found previously at PMO by Kumar et al. (2013) was probably a large regional global trend through North America to Europe (Cooper et al., 2014). Trend analyses for NO_x and NO_y are not shown here because the amount of qualified data for these species was not enough for an acceptable statistical test.

3.1.4. Transport affected by wildfire emissions
Transport affected by wildfire emissions ("Fire") occurred most frequently during summer when wildfires are more active. This transport pattern usually caused drastic changes in pollution levels at PMO due to the great amount of combustion emissions and fast transport in the free troposphere following the strong lifting created by large fires (Val Martín et al., 2006). The superimposed RT (**Figure 3c**) shows the main pathways from Canada to PMO, which are longer pathways from higher latitude than those of NA-anthro (**Figure 3b**). This region is fre-

quently dominated by persistent high pressure systems, which leads to dry climates in Canada and Alaska and increases the likelihood of wildfire occurrence in the regions (Macias Fauria and Johnson, 2006).

Boreal wildfires have been found to emit CO more intensively than anthropogenic activities and to cause significant O_3 production due to the large amount of CO emitted from large areas of vegetation burned in a short period of time (e.g., Parrington et al. (2013)). As shown in **Table 2**, the Fire transport pattern had an averaged CO mixing ratio of 108 ppbv, which was enhanced by 25 ppbv (30%) compared with the background (NATL). The enhancement was generally stronger than that caused by NA-anthro (14 ppbv, 17%) in summer. CO levels reported to represent fire signatures were different from those reported in previous studies (Val Martín et al., 2006, 2008a) because different methods were used in determining fire events. The average CO for fire events reported by Val Martín et al. (2006) was 139 ppbv, using a CO cutoff value of 110 ppbv in determining the events in 2004. Val Martín et al. (2008a) reported average CO of 124 ppbv and 105 ppbv, respectively, for fire affected periods in 2004 and 2005 at PMO using 75th percentiles of the FLEXPART_CO from fire emissions as the cutoff (compared to a fixed 15 ppbv of FLEXPART_CO used here). In spite of the differences, all studies indicated significant CO enhancements in transport of fire emissions. The enhancement of O_3 in fire plumes (16 ppbv, 50%) was also stronger than that in NA-anthro (10 ppbv, 32%) in summer. These facts suggest that fires act as a competing air pollution source to anthropogenic sources in the central North Atlantic, even though the frequency of Fire (7.3%) is about half of the frequency of NA-anthro in summer.

Vegetation fuel nitrogen can lead to high NO_x mixing ratios in fire plumes (Andreae and Merlet, 2001). The mixing ratios of NO_x and NO_y of Fire were higher than NATL by 9 pptv and 138 pptv, respectively, and these enhancements were in agreement with the values (9–30 pptv for NO_x, and 117–175 pptv for NO_y) reported by Val Martín

Zhang et al: Ten-year chemical signatures associated with long-range transport observed in the free troposphere over the central North Atlantic

Art. 8, page 11 of 20

et al. (2008a). The large enhancement of NO_y after long-rang transport could be due to chemical transformation of the nitrogen oxides in fire plumes. Through aircraft measurements, Alvarado et al. (2010) observed that 40% of the initial NO_x emissions were converted to PAN within a few hours in boreal biomass burning. Fast conversion of NO_x to NO_y may promote long-range transport of NO_y produced by wildfires.

3.1.5. Transport from the upper troposphere and lower stratosphere

Downward mixing from the UTLS ("Upper") had frequencies of 2.1–4.1%, with the highest frequency in fall. The fall maximum was likely caused by stratosphere-troposphere-exchange (STE) in the polar and middle latitude regions, which shifts southward from summer to winter (Holton et al., 1995). The transport pathways are shown in **Figure 3d**. A general transport direction from the northwest of PMO reflects the typical dynamics in anticyclones and tropopause folding in the mid-latitude.

The Upper transport pattern had CO means of 123, 92, and 96 ppbv for spring, summer, and fall, respectively (**Table 2**), which were ~10 ppbv higher than CO mixing ratios of NATL. CO has no large sources at high altitude and has been found to be mainly trapped in the lower troposphere (Liang et al., 2011). However, two potential reasons may lead to slight CO enhancement for the Upper transport pattern. In the superimposed RT plots of the two transport patterns, Upper and NATL, in **Figure 3a** and **3d**, air mass origins of Upper covered large sub-polar regions, while NATL covered the middle and low latitude regions. Air masses from the north should contain higher CO because of longer CO lifetime as a result of lower OH concentrations (Novelli et al., 1998). In addition, Upper transport also covered the whole boreal North American region (**Figure 3d**), so the Upper may also receive CO contributions from wildfires from that area.

The Upper transport had average O_3 mixing ratios of 58, 54, and 49 ppbv for spring, summer, and fall, respectively, which were the highest among all transport patterns. O_3 enhancement was ~20 ppbv, which is double that of NA-anthro. Such impact has been well recognized before and been associated with downward transport of naturally high O_3 in the UTLS (e.g., Logan, 1999; Neuman et al., 2012). The debate about stratospheric influence versus tropospheric production as the major source of tropospheric O_3 has existed for years (Monks et al., 2000). Subsidence of stratospheric ozone has been shown to have signification contributions to episodic ozone enhancements in the lower troposphere. Parrish et al. (1993) reported ozone enhancements (up to 60 ppbv) due to injection of stratospheric ozone at Cape Race, Canada. Springtime downward transport events were found to cause one-minute average ozone reaching 100 ppbv in Boulder, U.S., and a peak concentration of 215 ppbv in the Rocky Mountains (Langford et al., 2009). At an elevated site, Mount Washington, New Hampshire, U.S., a stratospheric influence was found to cause ozone enhancement in air flows associated with atmospheric anticyclones (Fischer et al., 2004). Although

we found downward transport caused the highest O_3 enhancements at PMO, the occurrence frequencies of this transport pattern (2.1%, 2.3% and 4.1%) were much lower than those of NA-anthro. Therefore, on an annual average basis, the total O_3 contribution from downward mixing was less significant than transport of anthropogenic pollution emissions. By comparing the products of the occurrence frequencies and O_3 enhancements associated to NA-anthro and Upper transport patterns, we estimated that the overall O_3 contribution by downward mixing is about 40% of the transport of anthropogenic emissions.

The Upper transport pattern also had the highest NO_x mixing ratios in all three seasons. The NO_x means were 63, 66, and 53 pptv in spring, summer, and fall, respectively, which were 15–41 pptv higher than those of the NATL. NO_x is produced in the UTLS with the source being the photochemical oxidation of N_2O. The NO_y means of Upper were 271, 234, and 229 pptv in spring, summer, and fall, respectively, which were all higher than NATL. The elevated NO_y during downward mixing can be attributed to accelerated hydrocarbon degradation followed by formation of PAN in stratosphere-troposphere air mass exchange (Liang et al., 2011). Hydrocarbon degradation accelerates because of increased OH production as a result of mixing of O_3-rich air from UTLS with moist tropospheric air in the downward transport. The higher NO_y could be due to downward transport of upper tropospheric air having a high ratio of PAN/NO_y, which, to some extent, reduces the rate of wet removal of NO_y. The subsequent PAN decomposition could have led to production of NO_x.

3.1.6. Transport affected by upslope flow

Upslope flow occurred 13–24% of the time, with the lowest frequency in summer. The seasonality found here is in agreement with the previous meteorological study at PMO, but has generally lower frequencies than that estimated for the period of 2004–2005 (4.2–37 % (Kleissl et al., 2007)). CO and O_3 in Upslope transport were statistically higher than NATL. This indicates upslope transport of local anthropogenic emissions to PMO. The Upslope transport had the lowest NO_y, which was likely due to efficient wet scavenging of NO_y during lifting (cloud condensation was predicted to take place for 30% of Upslope periods). The mixing ratios of *n*- and *i*-butane were found to be higher than the background in all seasons, which was likely due to butane being used as a primary domestic fuel on the island. Concentration enhancements of the butane isomers were higher in spring than the other seasons, possible due to increased butane usage as heating fuel in the cold spring.

3.2. Relationships of observed trace gases

Due to differences in chemical mechanisms and reaction rates, concentrations of trace gases change at different rates in long-range transport, which leads to recognizable relationships between observed trace gases at PMO. Such relationships are able to reflect chemical transformation history during long-range transport. For example, $d[O_3]/d[CO]$ values have been used to reflect O_3 production tendency based on the fact that CO has a much longer

Art. 8, page 12 of 20

Zhang et al: Ten-year chemical signatures associated with long-range transport observed in the free troposphere over the central North Atlantic

lifetime (a few months) compared with O_3 (lifetime of days to weeks) in the troposphere. During transport from North America to PMO, $d[O_3]/d[CO]$ changes mainly reflect O_3 chemistry in the absence of fresh emissions. Light NMHC (alkanes and alkynes) are detectable after transport from NA to PMO and are good tracers to study photochemical aging. Due to the differences in size and structure, different NMHC decay at varying reaction rates against OH. By examining the ratios between NMHC, the photochemical age of air masses can be estimated (McKeen and Liu, 1993). In the following sections, we examine these relationships in PMO observations with particular attention paid to two major transport patterns, NATL and NA-anthro.

3.2.1. d[O₃]/d[CO]
$d[O_3]/d[CO]$ was calculated as the reduced major axis (RMA) slope of the two species. RMA slope takes into account the variability in both x- and y-coordinates (Ayers, 2001); it is used as a proper tool for correlation analysis of observed trace gases. We present $d[O_3]/d[CO]$ grouped for the transport patterns, NATL, Fire, Upper, and NA-anthro, in spring, summer, and fall respectively (**Figure 5**). The data used in these analyses were uninterrupted observations for more than 12 hours. In this way, only prominent events were considered to fully include remarkable changes in CO and O_3, so that a clear and credible slope was more likely to be obtained. Yokelson et al. (2013) discussed how the ratio cannot be used to characterize source emissions and plume aging when mixing with air masses of different composition occurs (e.g., plume mixes with O_3-rich stratospheric air and then with clean marine boundary layer air). For this reason, we reported the statistical significance of the regression analyses. In cases of substantial changes in background air composition during transport, the significance of the regression will be low (high p-values).

$d[O_3]/d[CO]$ values for NA-anthro were 0.59 (spring, **Figure 5a**), 0.71 (summer, **Figure 5b**), and 0.45 (fall, **Figure 5c**) ppbv/ppbv, which were all lower than the values found in direct transport events to PMO, with slopes around 1.0 (Honrath et al., 2004; Zhang et al., 2014). The lower slopes in the current work were expected because events with long transport time were also included, which should be less intensive in O_3 production (lower positive $d[O_3]/d[CO]$). The values of $d[O_3]/d[CO]$ have been reported to be lower and relatively consistent at sites in the U.S. (0.20–0.37 ppbv/ppbv), which reflected a combination of aging processes of air pollutants and mixing with remote clean air mass during transport (Chin et al., 1994; Parrish et al., 1998; Mao and Talbot, 2004). Using the Tropospheric Emission Spectrometer retrievals on the Aura satellite, Hegarty et al. (2009) reported a spring slope value of 0.13 ppbv/ppbv in the free troposphere over the mid-latitude regions extending from North America to the North Atlantic. Interestingly, further into the North Atlantic ocean, higher slopes were found at PMO (Honrath et al. (2004) and this work) and Izana, Canary Islands (Cuevas et al., 2013).

The observations affected by wildfires had lower $d[O_3]/d[CO]$ values (slopes of 0.31 and 0.12 ppbv/ppbv

for summer and fall respectively) than NA-anthro. The lower values were likely due to large amounts of CO produced in biomass burning and lower NO_x/CO emission ratios compared with anthropogenic sources (McKeen et al., 2002; Lapina et al., 2006). In addition, production of O_3 and NO_2 can be suppressed in wildfire plumes due to reduction of sunlight by heavy aerosol loadings (Real et al., 2007; Verma et al., 2009; Parrington et al., 2013). This variation in $d[O_3]/d[CO]$ in fire-affected patterns was consistent with a previous MOZART study at PMO (Pfister et al., 2006), in which lower $d[O_3]/d[CO]$ values were also found during periods associated with higher relative contribution of fire tracers. Val Martín et al. (2006) calculated the O_3 enhancement indicator for fire plumes captured at PMO in a different method, which is the $\Delta[O_3]/\Delta[CO]$ (Δ refers to the difference between observed concentrations and an estimated background), and reported a similar mean value of 0.20 ppbv/ppbv for summer 2004.

The slopes for NATL were higher than NA-anthro in spring and fall. In both seasons, a few high O_3 mixing ratios (greater than 50 ppbv) were observed for NATL. We investigated those periods specifically and found that these events received ~9% RT from above 5 km. This suggested that NATL receives non-negligible contributions from UTLS in general, even though strict criteria were applied to ensure that the majority RT originated from the lower troposphere. As a result, occasionally high O_3 mixing ratios combined with low CO should be expected in the background of PMO. Examples of such observations are marked by gold dotted rectangles in **Figure 5a** and 5b. These observations show high O_3 concentrations (up to 60 ppbv) in the lower end of CO ranges in spring and summer, pull the regression toward higher slopes, and lead to low correlation coefficients. Positive $d[O_3]/d[CO]$ caused by downward mixing was also observed in a previous study using GEOS-Chem to interpret global satellite observations of $d[O_3]/d[CO]$ (Kim et al., 2013). Negative slopes indicating anticorrelation between O_3 and CO were found in winter at a few ground sites (Parrish et al., 1998; Macdonald et al., 2011), which were attributed to titration of O_3 by NO in emissions. Strong vertical mixing carrying air mass from the upper troposphere was also found to cause negative slopes (Fishman and Seiler, 1983).

3.2.2. Oxidation of butane isomers
Figure 6 shows the observed ratios of [i-butane]/[n-butane] as a function of [n-butane] for all paired observations in the ten years. Observations for NA-anthro and NATL are shown in colors as indicated by the legends. The geometric means (red symbols) and standard deviations (bars) for the two transport patterns are also shown. Mixing ratios of n-butane on the x-axis are given in a logarithmic scale to better display the wide range. The [i-butane]/[n-butane] values towards the left show a more scattered distribution because of lower precision of measurements near the detection limit. The [n-butane] mean for NA-anthro was higher than NATL as a result of emission influence. The means of [i-butane]/[n-butane] were both 0.49 for NA-anthro and NATL, and uncertainties were similar, which indicated no significant difference
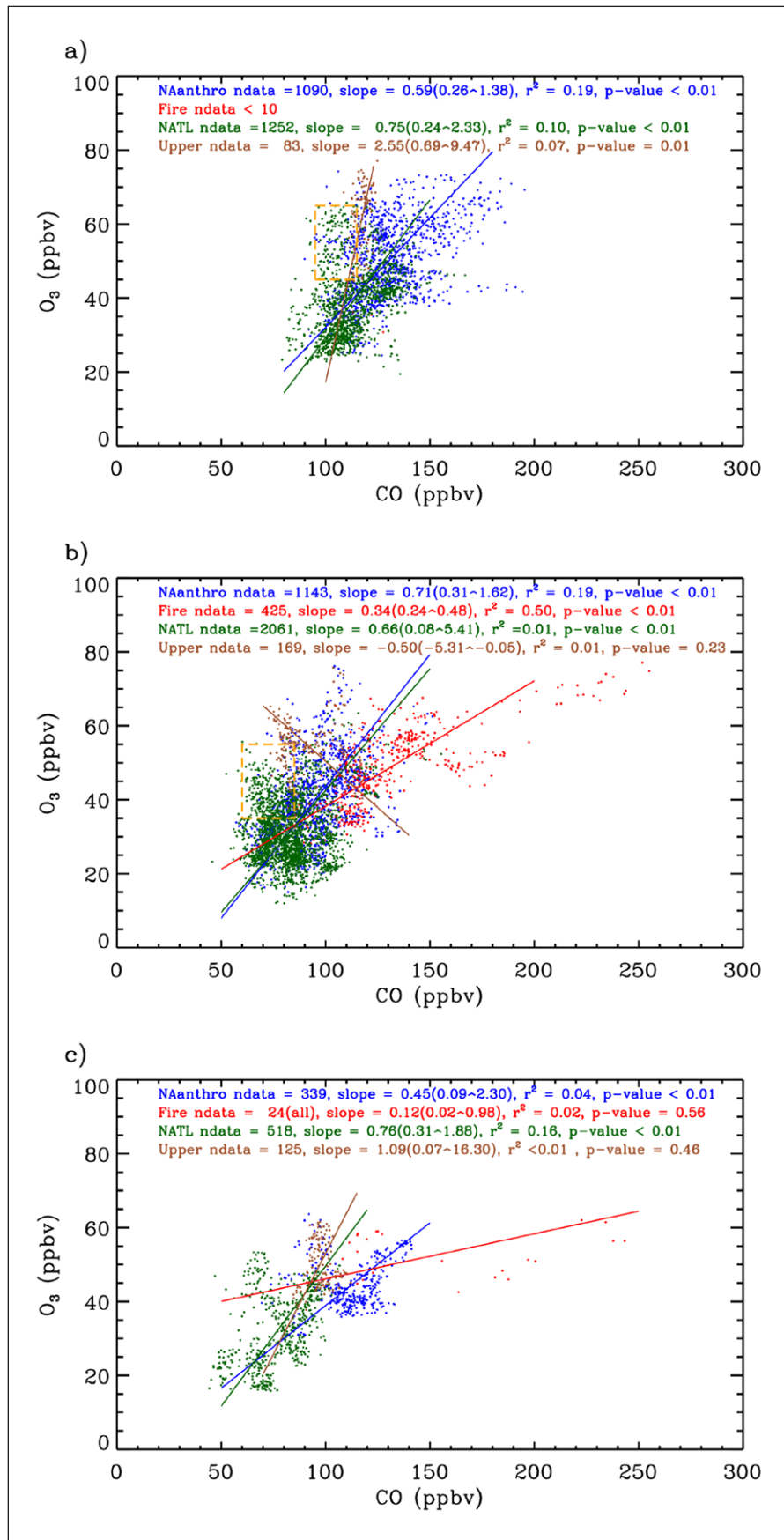
Zhang et al: Ten-year chemical signatures associated with long-range transport observed in the free troposphere over the central North Atlantic

Art.8, page 13 of 20

Figure 5: Regression analyses of observed O_3 and CO relationships for transport patterns NA-anthro, Fire, NATL, and Upper in spring **(a)**, summer **(b)**, and fall **(c)**. Only the observations of qualified continuous periods longer than 12 hour were used, except for the Fire transport pattern in fall, in which all observations were used. The gold dotted box marks observations likely influenced by subsidence air masses. See text for details. DOI: https://doi.org/10.1525/elementa.194.f5

Figure 6: Relationships between [i-butane]/[n-butane] and [n-butane] observed in all seasons. The black dots show the data for all available paired measurements (also including data that do not belong to any determined transport patterns). Observations for two patterns, including NATL and NAanthro, are color coded as described in the legends. Red symbols indicate the geometric means for the two patterns; error bars show the 25 and 75 percentiles of [i-butane]/[n-butane]. DOI: https://doi.org/10.1525/elementa.194.f6

in aging rates between butane isomers. Chlorine atoms have been found to cause faster oxidation of n-isomers in Arctic marine air (Hopkins et al., 2002). Chlorine atoms from oceanic sources were also found to affect NMHC observations in coastal regions during time periods when wind blows from the Pacific (Gorham et al., 2010). However, similar values of [i-butane]/[n-butane] were found at PMO in well-aged background air and transport of pollution, suggesting that the difference in oxidation speed for the butane isomers was hardly detectable. This implies that aging in both species is driven by OH, while other oxidants, such as Cl/Br, play minor roles. These results are in agreement with earlier findings by Helmig et al. (2008).

3.2.3. NMHC photochemical clock

Observed relationships between NMHC can be used to indicate atmospheric processing during long-range transport (i.e., photochemical aging and mixing with background air). The logarithmic ratio of NMHC pairs (i.e., (ln [n-butane]/[ethane])/(ln [propane]/[ethane])) is a function of both OH, and NMHC concentrations in emission sources (Parrish et al., 2007). This approach works better than studying NMHC concentrations alone, since the ratio reduces the large variations of NMHC concentrations in emissions. The NMHC ratios are very effective tracers to study pollution transport to PMO, because NMHC have low concentrations and no significant emission over the ocean (McKeen and Liu, 1993).

The analyses of ln[n-butane]/[ethane] vs ln[propane]/ [ethane] shown in **Figure 7** investigate photochemical aging and mixing extent during transport to PMO,

with specific attention paid to NATL and NA-anthro (**Figure 7b**). A kinetic scenario is an ideal condition, in which we assumed an isolated plume and no mixing with the marine air during transport. The kinetic scenario is indicated by the solid line with scales in both panels of **Figure 7**. The slope and aging scales were calculated using the same kinetic reaction rates as provided by Helmig et al. (2008) and an assumed constant [OH] of 1.0×10^6 molecule/cm^3. A global mean [OH] was chosen based on the estimate from Roelofs and Lelieveld (2000), but one should note that [OH] in the troposphere at northern midlatitudes has been found higher in spring than in summer and fall (Spivakovsky et al., 1990). For this reason, the intervals between age scales in **Figure 7** would be longer in spring and shorter in fall. The end point on the upper right of the kinetic line was defined by the NMHC ratios in continental emissions derived by Helmig et al. (2008). Data for NATL and NA-anthro are shown in different colors in the legends in **Figure 7**. Most data locate between the kinetic line and the mixing line indicating transport involved both aging and mixing processes. The regression of all data (solid line without scales) gave a RMA slope of 1.44 with $r^2 = 0.55$ and $p < 0.01$. The ten-year observation gave a range of the NMHC age at PMO from 7 to more than 20 days, with a mean of 11 days and a standard deviation of 4 days. This estimated mean age was greater than that found in previous studies at PMO using FLEXPART (Honrath et al., 2004; Zhang et al., 2014). Again, the reason was mainly that previous studies focused on a few efficient transport events, whereas all transport event candidates from North America are included here. The
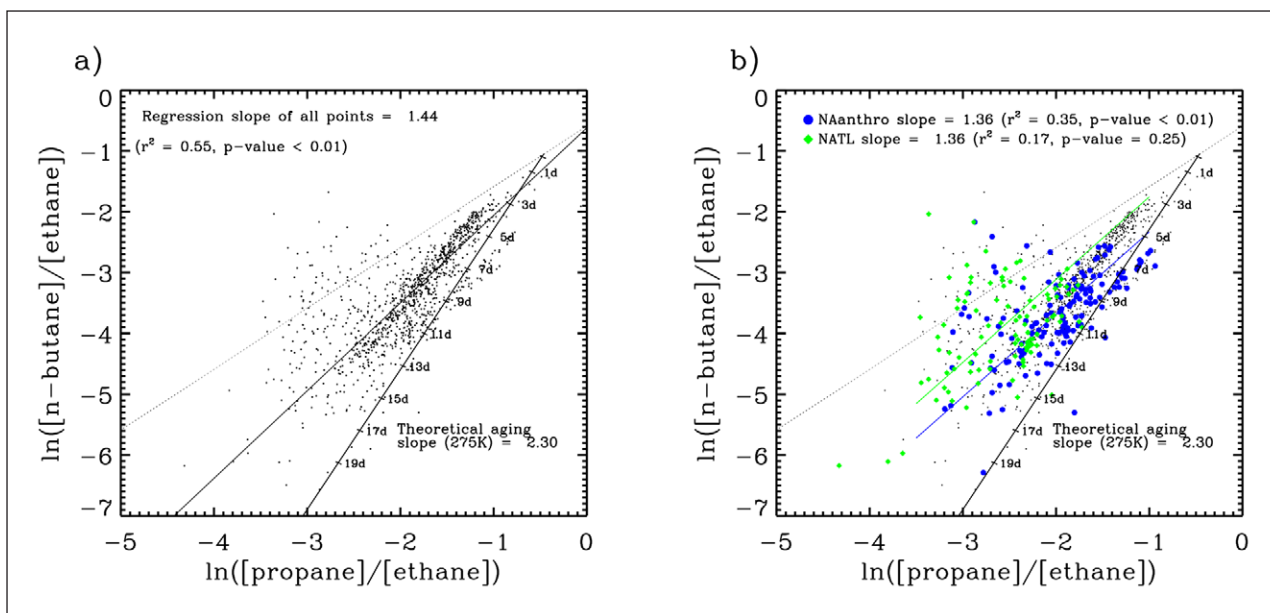
Zhang et al: Ten-year chemical signatures associated with long-range transport observed in the free troposphere over the central North Atlantic

Art. 8, page 15 of 20

Figure 7: Regression analyses of ln([n-butane]/[ethane]) and ln([propane]/[ethane]) relationships for all observations **(a)** and two transport patterns **(b)**, (NATL and NA-anthro). The dotted lines in both figures indicate the mixing-only trend initiated from an assumed origin (upper right end) based on concentrations in emissions. The solid lines with scales show the photochemical decay slope from the same origin for a fixed OH concentration defined in the text. In both figures, the black dots show the data for all available paired measurements (including data that do not belong to any defined transport patterns). The method to compute the slopes is discussed in the text. The legend provides, for all observations and the two transport patterns, linear regression slopes, correlation coefficients, and p values. DOI: https://doi.org/10.1525/elementa.194.f7

regression slope for NA-anthro was 1.36 with $r^2 = 0.35$, which is consistent with observations in previous studies for long-range transport over the North Atlantic (Parrish et al., 2007; Helmig et al., 2008). The estimated mean for NA-anthro was 11. 5 days with a standard deviation of 3.5 days. The NA-anthro mean was similar to the mean estimated based on all observations, suggesting a dominating influence of NA-anthro. There was a much less credible regression for NATL ($p = 0.25$), which was likely due to information loss on the source after extended aging. The estimated mean of NATL age was 15 days with a standard deviation of 3.5 days.

4. Summary and Conclusions
We categorized the dominant transport patterns to Pico Mountain Observatory for the years 2001–2010 by considering factors that affect air mass composition including types of emission sources, atmospheric RT, transport height, and upslope flow. FLEXPART and simulated meteorological conditions were used to quantify these factors. Observations of trace gases for the transport patterns, viewed as chemical signatures, were compared and discussed to investigate the characteristics of long-range transport to the central North Atlantic.

Trace gas concentrations at PMO were driven by both pollution emissions and natural sources. Anthropogenic emissions contributed an additional 14–23 ppbv (13%–28%) CO and ~10 ppbv (25%–30%) O_3 to background levels at PMO depending on the seasons. Wildfires caused even higher pollutant levels (25 ppbv (30%) CO and 16 ppbv (45%) of O_3) in summer, and were comparable

sources of trace gases to anthropogenic emissions. The O_3 enhancements caused by UTLS downward mixing were about two times that caused by North American anthropogenic emissions. Downward mixing also caused slight CO enhancements at PMO, which were likely due to transport from high latitudes where CO has a longer lifetime. Higher NO_x concentrations were found in transport from North America. Variations of the enhancements in different transport patterns were attributed to temperature and height dependent processes, such as wet scavenging and chemical reactions. High NO_y and O_3 were found in lifted transport from North America, which supports previous findings that PAN preserves O_3 production tendency after long-range transport. Highest NO_x was found in downward transport, likely a result of thermal decomposition of PAN in subsidence.

The slope $d[O_3]/d[CO]$ has been used as an indicator of O_3 production tendency, and it reflected O_3 chemistry and composition of original air masses. The values of $d[O_3]/d[CO]$ for Fire (0.12–0.33) were lower than those for NA-anthro and NATL, which was likely due to the much larger amount of CO emission from wildfires. The mixing with O_3-rich air masses creates largely varying O_3 within a narrow CO range, which tends to result in the high variability in $d[O_3]/d[CO]$. Remarkable downward mixing showed highly positive or negative $[O_3]/d[CO]$ values, likely due to the opposite vertical gradients of O_3 and CO, but the strength of the correlation was relatively low.

Mixing ratios of light NMHC were used to study oxidation processing during transport to PMO. The ratios of butane isomers for NATL and NA-anthro were not

Art. 8, page 16 of 20

Zhang et al: Ten-year chemical signatures associated with long-range transport observed in the free troposphere over the central North Atlantic

significantly different, which implies that sources signatures and oxidation rates were similar. Enhanced levels of butane isomers were observed during periods when upslope flow occurred, likely due to butane being used in the fuel on the Island. The average NMHC photochemical ages for NA-anthro and the entire dataset were 11.5 ± 3.5 and 11.0 ± 4.0 days. This estimate reflected the general air mass age for long-range transport to PMO and confirmed the dominating role of North American emissions.

5. Data accessibility statement

The following datasets were generated/used: PMO observations of trace gases and meteorology: available from website http://instaar.colorado.edu/pico/pico_archive/default.html FLEXPART simulations: available upon request due to large data files.

6. Acknowledgements

7. Funding Information

8. Competing Interests

Detlev Helmig is the Editor-in-Chief of the Elementa Atmospheric Science Domain. He was not involved in the peer review of the article.

9. Contributions

· Contributed to conception and design: B. Zhang, R. C. Owen, J. A. Perlinger, and D. Helmig.
· Contributed to acquisition of data: R. C. Owen, D. Helmig, M. Val Martín, L. Kramer, and B. Zhang.
· Contributed to analysis and interpretation of data: B. Zhang, R. C. Owen, J. A. Perlinger, and D. Helmig.
· Contributed to conducting FLEXPART simulations and model result analysis: B. Zhang and R. C. Owen.
· Drafted and/or revised the article: B. Zhang, R. C. Owen, J. A. Perlinger, D. Helmig, M. Val Martín, L. Kramer, L. R. Mazzoleni, and C. Mazzoleni.
· Approved the submitted version for publication: B. Zhang, R. C. Owen, J. A. Perlinger, D. Helmig, M. Val Martín, L. Kramer, L. R. Mazzoleni, and C. Mazzoleni.

References

Alvarado, MJ, Logan, JA, Mao, J, Apel, E, Riemer, D, Blake, D, Cohen, RC, Min, K-E, Perring, AE, Browne, EC, Wooldridge, PJ, Diskin, GS, Sachse, GW, Fuelberg, H, Sessions, WR, Harrigan, DL, Huey, G, Liao, J, Case-Hanks, A, Jimenez, JL, Cubison, MJ, Vay, SA, Weinheimer, AJ, Knapp, DJ, Montzka, DD, Flocke, FM, Pollack, IB, Wennberg, PO, Kurten, A, Crounse, J, Clair, JMS, Wisthaler, A, Mikoviny, T, Yantosca, RM, Carouge, CC and **Le Sager, P** 2010 Nitrogen oxides and PAN in plumes from boreal fires during ARC-TAS-B and their impact on ozone: an integrated analysis of aircraft and satellite observations, *Atmos. Chem. and Phys.,* **10**, 9739–9760. DOI: https://doi.org/10.5194/acp-10-9739-2010

Ambrose, J, Reidmiller, D and **Jaffe, D** 2011 Causes of high O 3 in the lower free troposphere over the Pacific Northwest as observed at the Mt. Bachelor Observatory, *Atmospheric Environment,* **45**, 5302–5315. DOI: https://doi.org/10.1016/j.atmosenv.2011.06.056

Andreae, MO and **Merlet, P** 2001 Emission of trace gases and aerosols from biomass burning, *Global biogeochemical cycles,* **15**, 955–966. DOI: https://doi.org/10.1029/2000GB001382

Ayers, G 2001 Comment on regression analysis of air quality data, Atmos. Environ., **35**, 2423–2425.

Beekmann, M, Ancellet, G and **Mégie, G** 1994 Climatology of tropospheric ozone in southern Europe and its relation to potential vorticity, *Journal of Geophysical Research: Atmospheres,* **99**, 12841–12853.

Bey, I, Jacob, DJ, Logan, JA and **Yantosca, RM** 2001 Asian chemical outflow to the Pacific in spring: Origins, pathways, and budgets.

Blake, NJ, Blake, DR, Sive, BC, Katzenstein, AS, Meinardi, S, Wingenter, OW, Atlas, EL, Flocke, F, Ridley, BA and **Rowland, FS** 2003 The seasonal evolution of NMHCs and light alkyl nitrates at middle to high northern latitudes during TOPSE, *Journal of Geophysical Research: Atmospheres,* **108**. DOI: https://doi.org/10.1029/2001jd001467

Brioude, J, Arnold, D, Stohl, A, Cassiani, M, Morton, D, Seibert, P, Angevine, W, Evan, S, Dingwell, A, and **Fast, JD** 2013 The Lagrangian particle dispersion model FLEXPART-WRF version 3.1, *Geoscientific Model Development,* **6**, 1889–1904. DOI: https://doi.org/10.5194/gmd-6-1889-2013

Carpenter, L, Green, T, Mills, G, Bauguitte, S, Penkett, S, Zanis, P, Schuepbach, E, Schmidbauer, N, Monks, P and **Zellweger, C** 2000 Oxidized nitrogen and ozone production efficiencies in the springtime free troposphere over the Alps, *Journal of Geophysical Research: Atmospheres,* **105**, 14547–14559.

Chin, M, Jacob, DJ, Munger, JW, Parrish, DD and **Doddridge, BG** 1994 Relationship of ozone and carbon monoxide over North America, *J. Geophys. Res.,* **99**, 14565–14573.

Zhang et al: Ten-year chemical signatures associated with long-range transport observed in the free troposphere over the central North Atlantic

Art. 8, page 17 of 20

China, S, Scarnato, B, Owen, RC, Zhang, B, Ampadu, MT, Kumar, S, Dzepina, K, Dziobak, MP, Fialho, P, Perlinger, JA, et al. 2015 Morphology and mixing state of aged soot particles at a remote marine free troposphere site: Implications for optical properties, *Geophys. Res. Lett.,* **42**, 1243–1250. DOI: https://doi.org/10.1002/2014GL062404

Cooper, OR, Gao, R-S, Tarasick, D, Leblanc, T and Sweeney, C 2012 Long-term ozone trends at rural ozone monitoring sites across the United States, 1990–2010, *J. Geophys. Res.: Atmos. (1984–2012),* 117.

Cooper, OR, Moody, JL, Parrish, DD, Trainer, M, Ryerson, TB, Holloway, JS, Hubler, G, Fehsenfeld, FC, Oltmans, SJ and Evans, MJ 2001 Trace gas signatures of the airstreams within North Atlantic cyclones: Case studies from the North Atlantic Regional Experiment (NARE '97) aircraft intensive, *J. Geophys. Res.,* **106**, 5437–5456. DOI: https://doi.org/10.1029/2000JD900574

Cooper, OR, Parrish, D, Ziemke, J, Balashov, N, Cupeiro, M, Galbally, I, Gilge, S, Horowitz, L, Jensen, N, Lamarque, J-F, et al. 2014 Global distribution and trends of tropospheric ozone: An observation-based review, Elementa: Science of the Anthropocene, **2**, 000–029.

Cuevas, E, González, Y, Rodríguez, S, Guerra, JC, Gómez-Peláez, AJ, Alonso-Pérez, S, Bustos, J, and Milford, C 2013 Assessment of atmospheric processes driving ozone variations in the subtropical North Atlantic free troposphere, *Atmos. Chem. and Phys.,* **13**, 1973–1998. DOI: https://doi.org/10.5194/acp-13-1973-2013

Dzepina, K, Mazzoleni, C, Fialho, P, China, S, Zhang, B, Owen, R, Helmig, D, Hueber, J, Kumar, S, Perlinger, J, et al. 2015 Molecular characterization of free tropospheric aerosol collected at the Pico Mountain Observatory: a case study with a long-range transported biomass burning plume, *Atmos. Chem. and Phys.,* **15**, 5047–5068. DOI: https://doi.org/10.5194/acp-15-5047-2015

Eckhardt, S, Stohl, A, Wernli, H, James, P, Forster, C, and Spichtinger, N 2004 A 15-year climatology of warm conveyor belts, *J. Climate,* **17**, 218–237. DOI: https://doi.org/10.1175/1520-0442(2004)017<0218:AYCOWC>2.0.CO;2

Emanuel, KA and Zivkovic-Rothman, M 1999 Development and evaluation of a convection scheme for use in climate models, *Journal of the Atmospheric Sciences,* **56**, 1766–1782. DOI: https://doi.org/10.1175/1520-0469(1999)056<1766:DAEOAC>2.0.CO;2

EPA 2016 Air Pollutant Emissions Trends Data, URL https://www.epa.gov/air-emissions-inventories/air-pollutant-emissions-trends-data, last accessed: November 2016.

Fehsenfeld, FC, Ancellet, G, Bates, TS, Goldstein, AH, Hardesty, RM, Honrath, R, Law, KS, Lewis, AC, Leaitch, R, McKeen, S, Meagher, J, Parrish, D, Pszenny, AAP, Russell, PB, Schlager, H, Seinfeld, J, Talbot, R and Zbinden, R 2006 International Consortium for Atmospheric Research on Transport and Transformation (ICARTT): North America to Europe – Overview of the 2004 summer field study, *J. Geophys. Res.,* **111**(D23), S01. DOI: https://doi.org/10.1029/2006JD007829

Fehsenfeld, FC, Trainer, M, Parrish, DD, VolzThomas, A and Penkett, S 1996 North Atlantic Regional Experiment 1993 summer intensive: Foreword, *J. Geophys. Res.,* **101**.

Fialho, P, Hansen, A and Honrath, R 2005 Absorption coefficients by aerosols in remote areas: a new approach to decouple dust and black carbon absorption coefficients using seven-wavelength Aethalometer data, *Journal of Aerosol Science,* **36**, 267–282. DOI: https://doi.org/10.1016/j.jaerosci.2004.09.004

Fischer, EV, Talbot, RW, Dibb, JE, Moody, JL and Murray, GL 2004 Summertime ozone at Mount Washington: Meteorological controls at the highest peak in the northeast, *J. Geophys. Res.,* **109**. DOI: https://doi.org/10.1029/2004jd004841

Fishman, J and Seiler, W 1983 Correlative nature of ozone and carbon monoxide in the troposphere: Implications for the tropospheric ozone budget, *J. Geophys. Res.,* **88**, 3662–3670, DOI: https://doi.org/10.1029/JC088iC06p03662

GDAS: NCEP Global Data Assimilation System, URL http://ready.arl.noaa.gov/gdas1.php, accessed: Nov., 2014.

Gorham, KA, Blake, NJ, VanCuren, RA, Fuelberg, HE, Meinardi, S and Blake, DR 2010 Seasonal and diurnal measurements of carbon monoxide and nonmethane hydrocarbons at Mt. Wilson, California: Indirect evidence of atomic Cl in the Los Angeles basin, *Atmos. Environ.,* **44**, 2271–2279. DOI: https://doi.org/10.1016/j.atmosenv.2010.04.019

Hegarty, J, Mao, H and Talbot, R 2009 Synoptic influences on springtime tropospheric O_3 and CO over the North American export region observed by TES, *Atmos. Chem. Phys.,* **9**, 3755–3776. DOI: https://doi.org/10.5194/acp-9-3755-2009

Helmig, D, Muñoz, M, Hueber, J, Mazzoleni, C, Mazzoleni, L, Owen, RC, Val-Martin, M, Fialho, P, Plass-Duelmer, C, Palmer, PI, et al. 2015 Climatology and atmospheric chemistry of the non-methane hydrocarbons ethane and propane over the North Atlantic, *Elementa: Science of the Anthropocene,* **3**, 000–054.

Helmig, D, Tanner, DM, Honrath, RE, Owen, RC and Parrish, DD 2008 Nonmethane hydrocarbons at Pico Mountain, Azores: 1. Oxidation chemistry in the North Atlantic region, *J. Geophys. Res.,* **113**. DOI: https://doi.org/10.1029/2007jd008930

Holton, JR, Haynes, PH, McIntyre, ME, Douglass, AR, Rood, RB and Pfister, L 1995 Stratosphere-troposphere exchange, *Rev. Geophys.,* **33**, 403–439. DOI: https://doi.org/10.1029/95RG02097

Honrath, RE, Hamlin, AJ and Merrill, JT 1996 Transport of ozone precursors from the Arctic troposphere to

Art. 8, page 18 of 20

Zhang et al: Ten-year chemical signatures associated with long-range transport observed in the free troposphere over the central North Atlantic

the North Atlantic region, *Journal of Geophysical Research: Atmospheres,* **101**, 29335–29351.

Honrath, RE, Helmig, D, Owen, RC, Parrish, DD and **Tanner, DM** 2008 Nonmethane hydrocarbons at Pico Mountain, Azores: 2. Event-specific analyses of the impacts of mixing and photochemistry on hydrocarbon ratios, *J. Geophys. Res.,* **113**(D20), S92. DOI: https://doi.org/10.1029/2008JD009832

Honrath, RE, Owen, RC, Val Martin, M, Reid, JS, Lapina, K, Fialho, P, Dziobak, MP, Kleissl, J and **Westphal, DL** 2004 Regional and hemispheric impacts of anthropogenic and biomass burning emissions on summertime CO and O$_3$ in the North Atlantic lower free troposphere, *J. Geophys. Res.,* **109**(D24), 310. DOI: https://doi.org/10.1029/2004JD005147

Hopkins, J, Jones, I, Lewis, A, McQuaid, J and **Seakins, P** 2002 Non-methane hydrocarbons in the Arctic boundary layer, *Atmos. Environ.,* **36**, 3217–3229. DOI: https://doi.org/10.1016/S1352-2310(02)00324-2

Hübler, G, Fahey, D, Ridley, B, Gregory, G and **Fehsenfeld, F** 1992 Airborne measurements of total reactive odd nitrogen (NO$_y$), *Journal of Geophysical Research: Atmospheres,* **97**, 9833–9850. DOI: https://doi.org/10.1029/91JD02326

Hudman, RC, Jacob, DJ, Cooper, OR, Evans, MJ, Heald, CL, Park, RJ, Fehsenfeld, F, Flocke, F, Holloway, J, Hubler, G, Kita, K, Koike, M, Kondo, Y, Neuman, A, Nowak, J, Oltmans, S, Parrish, D, Roberts, JM and **Ryerson, T** 2004 Ozone production in transpacific Asian pollution plumes and implications for ozone air quality in California, *J. Geophys. Res.,* **109**. DOI: https://doi.org/10.1029/2004jd004974

Kim, P, Jacob, D, Liu, X, Warner, J, Yang, K, Chance, K, Thouret, V and **Nedelec, P** 2013 Global ozone-CO correlations from OMI and AIRS: constraints on tropospheric ozone sources, *Atmos. Chem. and Phys.,* **13**, 9321–9335. DOI: https://doi.org/10.5194/acp-13-9321-2013

Kleissl, J, Honrath, RE, Dziobak, MP, Tanner, D, Martin, MV, Owen, RC and **Helmig, D** 2007 Occurrence of upslope flows at the Pico mountaintop observatory: A case study of orographic flows on a small, volcanic island, *J. Geophys. Res.,* **112**(D10), S35. DOI: https://doi.org/10.1029/2006JD007565

Koike, M, Kondo, Y, Kita, K, Takegawa, N, Masui, Y, Miyazaki, Y, Ko, M, Weinheimer, A, Flocke, F, Weber, R, et al. 2003 Export of anthropogenic reactive nitrogen and sulfur compounds from the East Asia region in spring, *Journal of Geophysical Research: Atmospheres,* **108**. DOI: https://doi.org/10.1029/2002jd003284

Kramer, L, Helmig, D, Burkhart, J, Stohl, A, Oltmans, S and **Honrath, RE** 2015 Seasonal variability of atmospheric nitrogen oxides and non-methane hydrocarbons at the GEOSummit station, Greenland, *Atmospheric Chemistry and Physics,* **15**, 6827–6849. DOI: https://doi.org/10.5194/acp-15-6827-2015

Kumar, A, Wu, S, Weise, M, Honrath, R, Owen, R, Helmig, D, Kramer, L, Val Martin, M and **Li, Q** 2013 Free-troposphere ozone and carbon monoxide over the North Atlantic for 2001–2011, *Atmos. Chem. and Phys.,* **13**, 12537–12547.

Langford, A, Aikin, K, Eubank, C and **Williams, E** 2009 Stratospheric contribution to high surface ozone in Colorado during springtime, *Geophys. Res. Lett.,* **36**. DOI: https://doi.org/10.1029/2009gl038367

Lapina, K, Honrath, RE, Owen, RC, Martin, MV and **Pfister, G** 2006 Evidence of significant large-scale impacts of boreal fires on ozone levels in the midlatitude Northern Hemisphere free troposphere, *Geophys. Res. Lett.,* **33**(L10), 815. DOI: https://doi.org/10.1029/2006GL025878

Liang, Q, Rodriguez, JM, Douglass, AR, Crawford, JH, Olson, JR, Apel, E, Bian, H, Blake, DR, Brune, W, Chin, M, Colarco, PR, da Silva, A, Diskin, GS, Duncan, BN, Huey, LG, Knapp, DJ, Montzka, DD, Nielsen, JE, Pawson, S, Riemer, DD, Weinheimer, AJ and **Wisthaler, A** 2011 Reactive nitrogen, ozone and ozone production in the Arctic troposphere and the impact of stratosphere-troposphere exchange, *Atmos. Chem. and Phys.,* **11**, 13181–13199. DOI: https://doi.org/10.5194/acp-11-13181-2011

Li, Q, Jacob, DJ, Munger, JW, Yantosca, RM and **Parrish, DD** 2004 Export of NOy from the North American boundary layer: Reconciling aircraft observations and global model budgets, *Journal of Geophysical Research: Atmospheres,* **109**.

Li, QB, Jacob, DJ, Bey, I, Palmer, PI, Duncan, BN, Field, BD, Martin, RV, Fiore, AM, Yantosca, RM, Parrish, DD, Simmonds, PG and **Oltmans, SJ** 2002 Transatlantic transport of pollution and its effects on surface ozone in Europe and North America, *J. Geophys. Res.,* **107**. DOI: https://doi.org/10.1029/2001jd001422

Logan, JA 1999 An analysis of ozonesonde data for the lower stratosphere: Recommendations for testing models, *J. Geophys. Res.,* **104**, 16151–16170. DOI: https://doi.org/10.1029/1999JD900216

Logan, JA, Prather, MJ, Wofsy, SC and **McElroy, MB** 1981 Tropospheric chemistry: A global perspective, *J. Geophys. Res.,* **86**, 7210–7254. DOI: https://doi.org/10.1029/JC086iC08p07210

Macdonald, A, Anlauf, K, Leaitch, W, Chan, E and **Tarasick, D** 2011 Interannual variability of ozone and carbon monoxide at the Whistler high elevation site: 20022006, *Atmos. Chem. Phys,* **11**, 11431–11446. DOI: https://doi.org/10.5194/acp-11-11431-2011

Macias Fauria, M and **Johnson, EA** 2006 Large-scale climatic patterns control large lightning fire occurrence in Canada and Alaska forest regions, *Journal of Geophysical Research: Biogeosciences,* **111**. DOI: https://doi.org/10.1029/2006jg000181

Mao, HT and **Talbot, R** 2004 O-3 and CO in New England: Temporal variations and relationships, *J. Geophys. Res.,* **109**.

Zhang et al: Ten-year chemical signatures associated with long-range transport observed in the free troposphere over the central North Atlantic

Art. 8, page 19 of 20

McKeen, S and **Liu, S** 1993 Hydrocarbon ratios and photochemical history of air masses, *Geophys. Res. Lett.,* **20**, 2363–2366. DOI: https://doi.org/10.1029/93GL02527

McKeen, S, Wotawa, G, Parrish, D, Holloway, J, Buhr, M, Hübler, G, Fehsenfeld, F and **Meagher, J** 2002 Ozone production from Canadian wildfires during June and July of 1995, *J. Geophys. Res.,* **107**, ACH-7. DOI: https://doi.org/10.1029/2001JD000697

Monks, PS, Salisbury, G, Holland, G, Penkett, SA and **Ayers, GP** 2000 A seasonal comparison of ozone photochemistry in the remote marine boundary layer, *Atmospheric Environment,* **34**, 2547–2561. DOI: https://doi.org/10.1016/S1352-2310(99)00504-X

Moxim, W, Levy, H and **Kasibhatla, P** 1996 Simulated global tropospheric PAN: Its transport and impact on NO_x, *Journal of Geophysical Research: Atmospheres,* **101**, 12621–12638. DOI: https://doi.org/10.1029/96JD00338

Mu, M, Randerson, JT, van der Werf, GR, Giglio, L, Kasibhatla, P, Morton, D, Collatz, GJ, DeFries, RS, Hyer, EJ, Prins, EM, Griffith, DWT, Wunch, D, Toon, GC, Sherlock, V and **Wennberg, PO** 2011 Daily and 3-hourly variability in global fire emissions and consequences for atmospheric model predictions of carbon monoxide, *J. Geophys. Res.,* **116**(D24), 303. DOI: https://doi.org/10.1029/2011JD016245

Neuman, JA, Trainer, M, Aikin, KC, Angevine, WM, Brioude, J, Brown, SS, de Gouw, JA, Dube, WP, Flynn, JH, Graus, M, Holloway, JS, Lefer, BL, Nedelec, P, Nowak, JB, Parrish, DD, Pollack, IB, Roberts, JM, Ryerson, TB, Smit, H, Thouret, V and **Wagner, NL** 2012 Observations of ozone transport from the free troposphere to the Los Angeles basin, *J. Geophys. Res.,* **117**. DOI: https://doi.org/10.1029/2011jd016919

Novelli, P, Masarie, K and **Lang, P** 1998 Distributions and recent changes of carbon monoxide in the lower troposphere, *J. Geophys. Res.,* **103**, 19015–19033.

Olivier, J and **Berdowski, J** 2001 The Climate System, A.A. Balkema, Swets and Zeitlinger.

Owen, RC, Cooper, OR, Stohl, A and **Honrath, RE** 2006 An analysis of the mechanisms of North American pollutant transport to the central North Atlantic lower free troposphere, *J. Geophys. Res.,* **111**(D23), S58. DOI: https://doi.org/10.1029/2006JD007062

Parrington, M, Palmer, PI, Henze, D, Tarasick, D, Hyer, E, Owen, RC, Helmig, D, Clerbaux, C, Bowman, K, Deeter, M, et al. 2012 The influence of boreal biomass burning emissions on the distribution of tropospheric ozone over North America and the North Atlantic during 2010, *Atmos. Chem. and Phys.,* **12**, 2077–2098. DOI: https://doi.org/10.5194/acp-12-2077-2012

Parrington, M, Palmer, PI, Lewis, AC, Lee, JD, Rickard, AR, Di Carlo, P, Taylor, JW, Hopkins, JR, Punjabi, S, Oram, DE, Forster, G, Aruffo, E, Moller, SJ, Bauguitte, SJ-B, Allan, JD, Coe, H and **Leigh, RJ** 2013 Ozone photochemistry in boreal biomass burning plumes, *Atmos. Chem.* *and Phys.,* **13**, 7321–7341. DOI: https://doi.org/10.5194/acp-13-7321-2013

Parrish, DD, Hahn, CJ, Williams, EJ, Norton, RB, Fehsenfeld, FC, Singh, HB, Shetter, JD, Gandrud, BW and **Ridley, BA** 1992 Indications of photochemical histories of Pacific air masses from measurements of atmospheric trace species at Point Arena, California, *J. Geophys. Res.,* **97**, 15883–15901.

Parrish, DD, Holloway, JS, Trainer, M, Murphy, PC, Forbes, GL and **Fehsenfeld, FC** 1993 Export of North American ozone pollution to the north Atlantic Ocean, *Science,* **259**, 1436–1439. DOI: https://doi.org/10.1126/science.259.5100.1436

Parrish, DD, Law, KS, Staehelin, J, Derwent, R, Cooper, OR, Tanimoto, H, Volz-Thomas, A, Gilge, S, Scheel, H-E, Steinbacher, M and **Chan, E** 2012 Long-term changes in lower tropospheric baseline ozone concentrations at northern mid-latitudes, *Atmos. Chem. and Phys.,* **12**, 11485–11504. DOI: https://doi.org/10.5194/acp-12-11485-2012

Parrish, DD, Stohl, A, Forster, C, Atlas, EL, Blake, DR, Goldan, PD, Kuster, WC and **de Gouw, JA** 2007 Effects of mixing on evolution of hydrocarbon ratios in the troposphere, *J. Geophys. Res.,* **112**. DOI: https://doi.org/10.1029/2006jd007583

Parrish, DD, Trainer, M, Holloway, JS, Yee, JE, Warshawsky, MS, Fehsenfeld, FC, Forbes, GL and **Moody, JL** 1998 Relationships between ozone and carbon monoxide at surface sites in the North Atlantic region, *J. Geophys. Res.,* **103**, 13357–13376. DOI: https://doi.org/10.1029/98JD00376

Pfister, GG, Emmons, LK, Hess, PG, Honrath, R, Lamarque, J-F, Val Martin, M, Owen, RC, Avery, MA, Browell, EV, Holloway, JS, Nedelec, P, Purvis, R, Ryerson, TB, Sachse, GW and **Schlager, H** 2006 Ozone production from the 2004 North American boreal fires, *J. Geophys. Res.,* **111**. DOI: https://doi.org/10.1029/2006jd007695

Randerson, J, Chen, Y, Werf, G, Rogers, B and **Morton, D** 2012 Global burned area and biomass burning emissions from small fires, *Journal of Geophysical Research: Biogeosciences,* **117**. DOI: https://doi.org/10.1029/2012jg002128

Real, E, Law, KS, Weinzierl, B, Fiebig, M, Petzold, A, Wild, O, Methven, J, Arnold, S, Stohl, A, Huntrieser, H, Roiger, A, Schlager, H, Stewart, D, Avery, M, Sachse, G, Browell, E, Ferrare, R and **Blake, D** 2007 Processes influencing ozone levels in Alaskan forest fire plumes during long-range transport over the North Atlantic, *J. Geophys. Res.,* **112**, 19. DOI: https://doi.org/10.1029/2006JD007576

Roelofs, G-J and **Lelieveld, J** 2000 Tropospheric ozone simulation with a chemistry- general circulation model: Influence of higher hydrocarbon chemistry, *Journal of Geophysical Research: Atmos.,* **105**, 22697–22712. DOI: https://doi.org/10.1002/qj.49708235418

Sheppard, P 1956 Airflow over mountains, Quart. J. Roy. Meteor. Soc., **82**, 528–529.

Spivakovsky, C, Yevich, R, Logan, J, Wofsy, S, McElroy, M and Prather, M 1990 Tropospheric OH in a three-dimensional chemical tracer model: An assessment based on observations of CH3CCl3, *J. Geophys. Res.,* **95**, 18441–18471.

Stohl, A, Hittenberger, M and Wotawa, G 1998 Validation of the Lagrangian particle dispersion model FLEXPART against large-scale tracer experiment data, *Atmos. Environ.,* **32**, 4245–4264. DOI: https://doi.org/10.1016/S1352-2310(98)00184-8

Stohl, A, Sodemann, H, Eckhardt, S, Frank, A, Seibert, P and Wotawa, G 2011 The Lagrangian particle dispersion model FLEXPART version 8.2, FLEXPART user guide, url: http://zardoz.nilu.no/flexpart/flexpart/flexpart82.pdf (March 14, 2012).

Talbot, R, Dibb, JE, Scheuer, E, Kondo, Y, Koike, M, Singh, H, Salas, L, Fukui, F, Ballenthin, J, Meads, R, et al. 1999 Reactive nitrogen budget during the NASA SONEX mission, *Geophysical Research Letters.* DOI: https://doi.org/10.1029/1999GL900589

Tanner, D, Helmig, D, Hueber, J and Goldan, P 2006 Gas chromatography system for the automated, unattended, and cryogen-free monitoring of C2 to C6 nonmethane hydrocarbons in the remote troposphere, *Journal of Chromatography A,* **1111**, 76–88. DOI: https://doi.org/10.1016/j.chroma.2006.01.100

Val Martín, M, Honrath, RE, Owen, RC and Lapina, K 2008a Large-scale impacts of anthropogenic pollution and boreal wildfires on the nitrogen oxides over the central North Atlantic region, *J. Geophys. Res.,* **113**. DOI: https://doi.org/10.1029/2007jd009689

Val Martín, M, Honrath, RE, Owen, RC and Li, QB 2008b Seasonal variation of nitrogen oxides in the central North Atlantic lower free troposphere, *J. Geophys. Res.,* **113**(D17), 307. DOI: https://doi.org/10.1029/2007JD009688

Val Martín, M, Honrath, RE, Owen, RC, Pfister, G, Fialho, P and Barata, F 2006 Significant enhancements of nitrogen oxides, black carbon, and ozone in the North Atlantic lower free troposphere resulting from North American boreal wildfires, *J. Geophys. Res.,* **111**(D23), S60. DOI: https://doi.org/10.1029/2006JD007530

Verma, S, Worden, J, Pierce, B, Jones, DBA, Al-Saadi, J, Boersma, F, Bowman, K, Eldering, A, Fisher, B, Jourdain, L, Kulawik, S and Worden, H 2009 Ozone production in boreal fire smoke plumes using observations from the Tropospheric Emission Spectrometer and the Ozone Monitoring Instrument, *J. Geophys. Res.,* **114**. DOI: https://doi.org/10.1029/2008jd010108

Vogelezang, D and Holtslag, A 1996 Evaluation and model impacts of alternative boundary-layer height formulations, *Boundary-Layer Meteorology*, **81**, 245–269. DOI: https://doi.org/10.1007/BF02430331

Worden, HM, Deeter, MN, Frankenberg, C, George, M, Nichitiu, F, Worden, J, Aben, I, Bowman, KW, Clerbaux, C, Coheur, PF, de Laat, ATJ, Detweiler, R, Drummond, JR, Edwards, DP, Gille, JC, Hurtmans, D, Luo, M, Martinez-Alonso, S, Massie, S, Pfister, G, and Warner, JX 2013 Decadal record of satellite carbon monoxide observations, *Atmos. Chem. and Phys.,* **13**, 837–850. DOI: https://doi.org/10.5194/acp-13-837-2013

Yienger, J, Carmichael, G and Klonecki, A 1999 An evaluation of chemistry's role in the winter-spring ozone maximum found in the northern mid-latitude free troposphere, *Journal of geophysical research,* **104**, 3655–3667. DOI: https://doi.org/10.1029/1998JD100043

Yokelson, RJ, Burling, IR, Gilman, J, Warneke, C, Stockwell, CE, Gouw, Jd, Akagi, S, Urbanski, S, Veres, P, Roberts, JM, et al. 2013 Coupling field and laboratory measurements to estimate the emission factors of identified and unidentified trace gases for prescribed fires, *Atmospheric Chemistry and Physics,* **13**, 89–116. DOI: https://doi.org/10.5194/acp-13-89-2013

Zhang, B, Owen, RC, Perlinger, J, Kumar, A, Wu, S, Val Martin, M, Kramer, L, Helmig, D and Honrath, R 2014 A semi-Lagrangian view of ozone production tendency in North American outflow in the summers of 2009 and 2010, *Atmos. Chem. and Phys.,* **14**, 2267–2287. DOI: https://doi.org/10.5194/acp-14-2267-2014

ELEMENTA
Science of the Anthropocene

Elem Sci Anth is a peer-reviewed open access journal published by University of California Press.

OPEN ACCESS